Annals of Physics 347 (2014) 141–169

Contents lists available at ScienceDirect

Annals of Physics

journal homepage: www.elsevier.com/locate/aop

Deformation properties of the projected spherical single particle basis

A.A. Raduta [a,b,*,1], R. Budaca [a]

[a] Institute of Physics and Nuclear Engineering, Bucharest, POB MG6, Romania
[b] Academy of Romanian Scientists, 54 Splaiul Independentei, Bucharest 050094, Romania

HIGHLIGHTS

- The proposed model describes the properties of spherical and deformed nuclei in a unified fashion.
- The single particle energies corresponding to the projected spherical basis depend on the nuclear deformation.
- The basis can be used to treat many body systems.
- Analytical expression for the k-pole density is given.
- Comparisons with the Nilsson model, projected shell model and particle–rotor model are in detail discussed.

ARTICLE INFO

Article history:
Received 20 January 2014
Accepted 3 May 2014
Available online 10 May 2014

Keywords:
Angular momentum projection
Mean field
Single particle basis
Single particle energies
Nilsson model
Unified description

ABSTRACT

Deformed single particle energies obtained by averaging a particle–core Hamiltonian with a projected spherical basis depend on a deformation parameter and an arbitrary constant defining the canonical transformation relating the collective quadrupole coordinates and momenta with the boson operators. When the mentioned basis describes the single particle motion of either protons or neutrons the parameters involved are isospin dependent. An algorithm for fixing these parameters is formulated and then applied for 194 isotopes covering a good part of the nuclide chart. Relation with the Nilsson deformed basis is pointed out in terms of deformation dependence of the corresponding single particle energies as well as of the nucleon densities and their symmetries. The proposed projected spherical basis provides an efficient tool for the description of spherical and deformed nuclei in a unified fashion.

* Corresponding author at: Institute of Physics and Nuclear Engineering, Bucharest, POB MG6, Romania.
E-mail address: raduta@ifin.nipne.ro (A.A. Raduta).

[1] Senior Fellow of the Humboldt Foundation.

http://dx.doi.org/10.1016/j.aop.2014.05.001
0003-4916/

1. Introduction

Nuclear structure formalisms describe the spectroscopic properties either in terms of single particle degrees of freedom [1–8] or by using phenomenological collective coordinates [9–22]. Many attempts have been made to define the collective variables in terms of particle motion. The accuracy in treating a many body Hamiltonian depends on the single particle basis which is used. For example the essential features of the deformed nuclei cannot be described with a spherical single particle basis, unless this is of very large dimension. The shape of the mean field which defines the single particle motion should be consistent with the nuclear shape. In this context we should stress on the usefulness of the bases provided by the Nilsson model or the deformed Woods–Saxon interaction. Using a deformed single particle basis in a many body treatment like, Hartree–Bogoliubov procedure, quasiparticle random phase approximation (QRPA), higher QRPA methods, finally one obtains deformed many body functions and energies. Further the deformed wave functions are used to calculate matrix elements describing various physical processes. Since the experimental data to be described are obtained in the laboratory frame, the rotational symmetries have to be restored [23–37]. The angular momentum projection from a many body state is not an easy task, only few complicated codes being available. To simplify the projection operation the variational principle is used to find the energies of the ground band states. This approximation has the drawback that for high angular momentum where the angular momentum fluctuation is large, the description is of course unrealistic [38]. Moreover, it is difficult to extend the procedure to the excited bands.

About two decades ago, one of the authors (A. A. R.) proposed, in collaboration, an alternative way to describe the deformed nuclear systems [39]. Indeed, a projected spherical single particle basis has been constructed which allows for a unified description of spherical and deformed nuclei. It is amazing that although the projected single particle states have good rotational symmetry, the matrix elements of particle operators incorporate the deformation via a deformed core which is described by an axially symmetric coherent state defined with one component of the quadrupole boson. Many interesting properties have been described in several papers and moreover the basis has been successfully used to treat various processes.

However nowhere the involved parameters were discussed in a systematic manner and moreover a confident algorithm to fix them is not yet available. Also, it is interesting to see whether this basis can be related in some way to the one yielded by the Nilsson model. Of course one expects to depict certain fingerprints of deformation also in the nucleon density.

The above mentioned issues will be considered in next sections as follows: In Section 2, the projected spherical Nilsson's states and the corresponding single particle energies are defined. A projected spherical particle–core basis is introduced in Section 3. Therein one proves that such a basis could be used as a basis in the particle space. The connection with the projected Nilsson's basis is discussed both numerically and analytically. The fitting procedure of the parameters involved is described in detail in Section 4.

Numerical results regarding the fitting procedure are given in Section 5 for 194 isotopes. Here we also compare the shell filling and the nucleon densities yielded by the projected spherical and Nilsson's bases. The final conclusions are drawn in Section 6.

2. Projected Nilsson basis

To describe the single-particle motion in deformed nuclei one usually uses a quadrupole deformed mean-field which is simulated by an anisotropic harmonic oscillator potential. Such a potential can be understood as the average field describing the motion of a particle around an ellipsoidal core. Therefore the shell model Hamiltonian is replaced by

$$H = -\frac{\hbar^2}{2m}\Delta + \frac{m\omega_0^2}{2}\left(\Omega_\perp^2\rho^2 + \Omega_z^2 z^2\right) + C\vec{l}\cdot\vec{s} + D\vec{l}^2, \tag{2.1}$$

where the cylindrical coordinates are used. The deformation of the spherical equipotential surface to an ellipsoidal shape is performed with the restriction that the enclosed volume is preserved. This

condition is automatically satisfied by few parameterizations of the frequencies $\Omega_\perp$ and Ω_z. The one adopted here:

$$\Omega_\perp = \left(\frac{2+\delta}{2-\delta}\right)^{1/3}, \qquad \Omega_z = \left(\frac{2+\delta}{2-\delta}\right)^{-2/3}, \tag{2.2}$$

is different from that used by the Nilsson model [3],

$$\Omega_\perp^2 = 1+\frac{2}{3}\delta, \qquad \Omega_z^2 = 1-\frac{4}{3}\delta, \tag{2.3}$$

which is actually the first order approximation of (2.2). Our choice is justified by the fact that in the former case the oscillator frequency is the same as in the spherical limit, while the latter case requires a renormalization through a deformation dependent term. Note that the deformation parameter δ can be linked to the more popular deformation β through the relation $\delta = \sqrt{\frac{45}{16\pi}}\beta$.

With the parameterization (2.2), the Hamiltonian (2.1) can be rewritten as:

$$H_{Nilsson} = \hbar\omega_0\left[\frac{1}{2}\left(-\Delta'^2 + r'^2\right) + \frac{1}{2}V_1 r'^2 + V_2 r'^2 Y_{20}\right] + C\vec{l}\cdot\vec{s} + D\vec{l}^2, \tag{2.4}$$

where one used the stretched coordinates $r' = \sqrt{\alpha}r$ with $\alpha = \frac{m\omega_0}{\hbar}$ and the notations:

$$V_1 = -1 + \frac{1}{3}\Omega_z^2 + \frac{2}{3}\Omega_\perp^2, \tag{2.5}$$

$$V_2 = -\sqrt{\frac{\pi}{5}}\frac{2}{3}\left(\Omega_\perp^2 - \Omega_z^2\right). \tag{2.6}$$

The eigenvalues of this Hamiltonian, obtained by diagonalization, depend on deformation and so do the eigenstates:

$$|\Omega^\pi\alpha\rangle = \sum_{N,l,j} C^\alpha_{Nlj}(\delta)|Nlj\Omega\rangle. \tag{2.7}$$

Here Ω is the projection of the single-particle angular momentum j on the z axis, π is the parity while $N = 2n + l$ with n and l being the principal quantum number and the orbital angular momentum, respectively. For a given Ω^π the solutions provided by diagonalization are labeled by the completeness quantum number α. If one neglects the $\Delta N = 2$ interaction matrix elements, then the eigenstates are

$$|N\Omega\alpha\rangle = \sum_j C^\alpha_j(\delta)|Nlj\Omega\rangle. \tag{2.8}$$

Finally, projecting out the angular momentum from the state defined above, one recovers the spherical shell model state $|Nlj\Omega\rangle$. Therefore, in the angular momentum projected Nilsson model the single-particle energies are given by the diagonal matrix elements of the Hamiltonian (2.4) corresponding to the projected states $|Nlj\Omega\rangle$,

$$\begin{aligned}
\varepsilon^{Nilss}_{nlj\Omega} &= \langle Nlj\Omega|H_{Nilsson}|Nlj\Omega\rangle \\
&= \varepsilon_{nlj} + \hbar\omega_0 V_2\left(N+\frac{3}{2}\right)\sqrt{\frac{5}{4\pi}}C^{j2j}_{\Omega 0\Omega}C^{j2j}_{\frac{1}{2}0\frac{1}{2}} + \frac{1}{2}\hbar\omega_0 V_1\left(N+\frac{3}{2}\right) \\
&= \varepsilon_{nlj} - \hbar\omega_0\left(N+\frac{3}{2}\right)C^{j2j}_{\Omega 0\Omega}C^{j2j}_{\frac{1}{2}0\frac{1}{2}}\frac{\left(\Omega_\perp^2-\Omega_z^2\right)}{3} \\
&\quad + \frac{1}{2}\hbar\omega_0\left(-1+\frac{1}{3}\Omega_z^2+\frac{2}{3}\Omega_\perp^2\right)\left(N+\frac{3}{2}\right).
\end{aligned} \tag{2.9}$$

ε_{nlj} is the spherical shell model single-particle energy.

3. The projected particle–core product basis

The mean field that defines the single-particle motion approximates the interaction of a single particle with the rest of the particles which can be assimilated with a phenomenological core. Supposing that the spherical limit of the mean field is the spherical shell model single-particle Hamiltonian H_{SM}, the particle–core Hamiltonian is defined as:

$$H_{pc} = H_{core} + H_{SM} - m\omega_0^2 r^2 \sum_{\lambda=0,2} \sum_{\mu=-\lambda}^{\lambda} \alpha^*_{\lambda\mu} Y_{\lambda\mu}, \tag{3.1}$$

where

$$H_{core} = \omega_b \sum_{\mu} b^\dagger_{2\mu} b_{2\mu} \tag{3.2}$$

is a harmonic quadrupole boson Hamiltonian associated with the phenomenological core. The particle–core interaction represented by the last term, depends on the nuclear deformation through the monopole and quadrupole shape coordinates, α_{00} and $\alpha_{2\mu}$. The latter ones are related to the boson operators $b^\dagger_{2\mu}$ defining the harmonic oscillation of the core, through a canonical transformation

$$\alpha_{2\mu} = \frac{1}{\sqrt{2}k}\left[b^\dagger_{2\mu} + (-)^\mu b_{2\mu}\right], \quad -2 \le \mu \le 2, \tag{3.3}$$

which is defined up to an arbitrary constant k, at our disposal. The restriction of volume conservation provides a relation between the monopole and quadrupole coordinates:

$$\alpha_{00} = -\frac{1}{\sqrt{4\pi}} \sum_{\mu} \left|\alpha_{2\mu}\right|^2, \tag{3.4}$$

whose boson representation is

$$\alpha_{00} = -\frac{1}{4\sqrt{\pi}k^2}\left\{5 + \sum_{\mu}\left[2b^\dagger_{2\mu}b_{2\mu} + \left(b^\dagger_{2\mu}b^\dagger_{2-\mu} + b_{2-\mu}b_{2\mu}\right)(-)^\mu\right]\right\}. \tag{3.5}$$

Averaging H_{pc} on the eigenstates $|nljm\rangle$ of H_{SM} one obtains a deformed boson Hamiltonian whose ground state is described by a coherent state:

$$\psi_g = e^{d\left(b^\dagger_{20} - b_{20}\right)}|0\rangle_b, \tag{3.6}$$

where $|0\rangle_b$ is the vacuum state of the boson operators, while d is a real parameter which simulates the nuclear deformation. On the other hand, the average of H_{pc} with ψ_g is a single particle Hamiltonian, similar to that of the Nilsson model [3]:

$$H_{mf} = \langle\psi_g|H_{pc}|\psi_g\rangle = \omega_b d^2 + H_{SM} - \hbar\omega_0 r'^2\left[\frac{\sqrt{2}d}{k}Y_{20} - \frac{1}{8\pi k^2}(5 + 4d^2)\right], \tag{3.7}$$

where the stretched coordinates are used. Further, extracting from the above Hamiltonian the zero point deformation energy

$$\lim_{d\to 0}(H_{mf} - H_{SM}) = \frac{5\hbar\omega_0 r'^2}{8\pi k^2}, \tag{3.8}$$

one arrives at a more recognizable form:

$$H_{mf} = \omega_b d^2 + H_{SM} - \hbar\omega_0 r'^2\left(\frac{\sqrt{2}d}{k}Y_{20} - \frac{1}{2\pi k^2}d^2\right). \tag{3.9}$$

We note that the deformed terms involved in the Nilsson model Hamiltonian and the mean field H_{mf} are identical provided the following equation holds:

$$\frac{d}{k} = \frac{\beta}{\sqrt{2}}. \tag{3.10}$$

One recovers the original Nilsson Hamiltonian [3]:

$$H_{Nilsson}(\beta) = H_{SM} - \hbar\omega_0 r'^2 \beta Y_{20} \tag{3.11}$$

if in (3.9) one ignores the constant terms i.e., those which are independent of the particle coordinates.

Concluding, once the coordinates associated to one of the particle–core factor functions are frozen, the rotational symmetry is broken and a mean field for the motion of the unfrozen degree of freedom is obtained. We may use the mean field to define a new single particle basis which could further be involved in a many body calculation. Since the measured data have the symmetries specific to laboratory frame, we have to project out the good angular momentum from the many body state which, as a matter of fact, is not an easy task.

Our proposal [39] was to treat the particle–core system, which is rotationally invariant, with the projected states:

$$\Phi^{IM}_{nlj}(d) = \mathcal{N}^I_j P^I_{MI}\left[|nljI\rangle\Psi_g\right], \tag{3.12}$$

which form a basis for the particle–core space. Note that the unprojected particle–core state involved in (3.12) is a product function of the eigenstates of H_{SM} and $\langle nljm|H_{pc}|nljm\rangle$, respectively. In this way we assume that the deformation is carried only by the core. At this level the single particle factor state preserves the rotational symmetry, the deformation of the single particle motion being determined due to the interaction with the core. The tensorial form of this state,

$$\Phi^{IM}_{nlj}(d) = \mathcal{N}^I_j \sum_J C^{jJI}_{I\,0\,I}\left[N^{(c)}_J\right]^{-1}\left[|nlj\rangle\phi^{(c)}_J\right]_{IM}, \tag{3.13}$$

is often used for analytical calculations. Here we used the notation

$$\phi^{(c)}_{JM} = N^{(c)}_J P^J_{M0}\psi_g, \tag{3.14}$$

for the angular momentum projected coherent state, which is the ground band model state within the coherent state model (CSM) [19,20]. The norm of this state

$$\left[N^{(c)}_J\right]^{-2} = (2J+1)I^{(0)}_J e^{-d^2}, \tag{3.15}$$

as well as the corresponding matrix elements of any boson polynomial is expressed in terms of the overlap integrals:

$$I^{(k)}_J = \frac{d^k I^{(0)}_J}{dx^k}, \qquad I^{(0)}_J(x) = \int_0^1 P_J(y)e^{xP_2(y)}dy, \quad x = d^2, \tag{3.16}$$

where $P_J(y)$ denotes the Legendre polynomial of rank J. These integrals have been analytically calculated in Refs. [19,20]. Knowing the norm of the core projected state, one can write down the norm of the total particle–core state (3.12) as

$$\left(\mathcal{N}^I_j\right)^{-2} = \sum_J \left(C^{jJI}_{I\,0\,I}\right)^2\left[N^{(c)}_J\right]^{-2}. \tag{3.17}$$

We mention the fact that the limit of Φ^{IM}_{nlj} when $d \to 0$ exists even though the norms (3.17) for $j \neq I$, in the same limit, are indeterminate. Besides the orthogonality and other properties discussed in Refs. [39,40], one of the most important property of the basis (3.12) is that for vanishing deformation d it recovers the full spherical shell model basis described by the product state $|nljM\rangle|0\rangle_b$.

In general, i.e. for any deformation parameter this basis, although defined in the particle–core space, can be used as a single particle basis. This assertion is hinging on the fact that when the matrix element of a particle-like operator is calculated, one integrates first on core's coordinates, which results in generating

a deformation of the matrix element corresponding to the spherical shell model state. An example, on this line, concerns the single particle energies, which compared with those of projected Nilsson model proves that the deformation induced in this process is the appropriate one.

3.1. Energies

Since the core contribution does not depend on the single-particle quantum numbers, the single-particle energies of the mean field defined by the particle–core Hamiltonian (3.1) are given in the first order of perturbation by the average of $H_{pc}-H_{core}$ on the projected single-particle basis (3.12):

$$\begin{aligned}\varepsilon^I_{nlj} &= \langle\Phi^{IM}_{nlj}(d)|\left(H_{pc}-H_{core}\right)|\Phi^{IM}_{nlj}(d)\rangle\\ &= \varepsilon_{nlj}-\hbar\omega_0\left(N+\frac{3}{2}\right)\sqrt{\frac{5}{4\pi}}C^{j2j}_{I0I}C^{j2j}_{\frac{1}{2}0\frac{1}{2}}\frac{d\sqrt{2}}{k}\\ &\quad+\hbar\omega_0\left(N+\frac{3}{2}\right)\left[1+\frac{5}{2d^2}+\frac{\sum_J\left(C^{jIJ}_{I-I0}\right)^2 I^{(1)}_J}{\sum_J\left(C^{jIJ}_{I-I0}\right)^2 I^{(0)}_J}\right]\frac{d^2}{4\pi k^2}.\end{aligned} \tag{3.18}$$

Given the fact that the basis (3.12) recovers the spherical shell model basis in the vibrational limit, the corresponding single-particle energies (3.18) have also to reproduce the spherical shell model energy in the limit of $d\to 0$. However the limit

$$\lim_{d\to 0}\varepsilon^I_{nlj}=\varepsilon_{nlj}+\hbar\omega_0\left(N+\frac{3}{2}\right)\left[\frac{5}{2}+\frac{1}{2}\left[j-I+\frac{1}{2}\left(1-(-)^{j-I}\right)\right]\right]\frac{1}{4\pi k^2},\quad j\neq I, \tag{3.19}$$

is different from ε_{nlj} by the $1/k^2$ term in the above equation which is actually a measure of the so called *zero point energy*. The deviation is very small due to the constant k whose usual value varies around 10. However, at high j orbitals the correction becomes sizable and a split of the energy correction over the quantum number I, shows up at vanishing deformation. In order to avoid this one must normalize the single-particle energies (3.18) by extracting a zero point deformation energy given by the correction term from (3.19). Thus, the normalized single-particle energies are expressed as

$$\begin{aligned}\varepsilon^I_{nlj}(d;k) &= \varepsilon_{nlj}-\hbar\omega_0\left(N+\frac{3}{2}\right)\sqrt{\frac{5}{4\pi}}C^{j2j}_{I0I}C^{j2j}_{\frac{1}{2}0\frac{1}{2}}\frac{d\sqrt{2}}{k}\\ &\quad+\hbar\omega_0\left(N+\frac{3}{2}\right)\left[1+\frac{\sum_J\left(C^{jIJ}_{I-I0}\right)^2 I^{(1)}_J}{\sum_J\left(C^{jIJ}_{I-I0}\right)^2 I^{(0)}_J}\right]\frac{d^2}{4\pi k^2}\\ &\quad-\hbar\omega_0\left(N+\frac{3}{2}\right)\left[j-I+\frac{1}{2}\left(1-(-)^{j-I}\right)\right]\frac{1}{8\pi k^2}.\end{aligned} \tag{3.20}$$

Apart from deformation parameter d these single-particle energies depend on the canonical transformation constant k which can be fixed by fitting a collective observable as will be shown in the next section. The dependence on the deformation of the proton and neutron single-particle energies (3.20) for a fixed value of k is presented in Fig. 1. The shell model parameters κ and μ used there are taken from Ref. [15] and correspond to the majority of the rare earth nuclei.

Few words about the role of the constant k are necessary. The plots of Fig. 1 are sensible to the variation of k. Indeed, increasing k the energy curves approach straight lines. One can say that k plays the role of a scaling parameter. Indeed, the leading term in deformation depend on the quantity d/k rather on the deformation d alone. This is also true for the quadratic term, because the ratio of the overlap integrals is a fractional quantity and thus a scalable one, at least in the extreme limits of vibrational and asymptotic regimes.

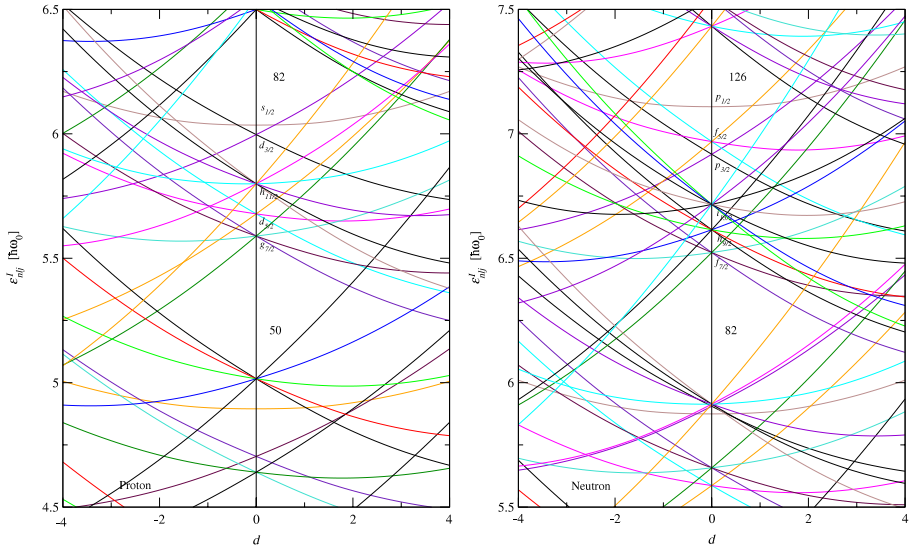

Fig. 1. Proton and neutron single-particle energies in the region of $N = 5$ and $N = 6$ shells respectively, given by Eq. (3.20) where the shell model parameters $\kappa = 0.0637$ and $\mu = 0.60$ for protons and $\mu = 0.42$ for neutrons were used. The canonical transformation constant is fixed to $k = 10$.

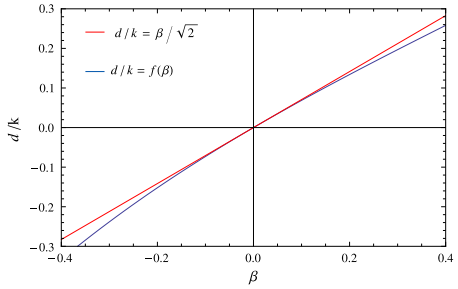

Fig. 2. The ratio d/k given as a function of the nuclear deformation β according to the linear dependence (3.10) and the more complex one given by Eq. (3.21).

The averages (3.20) can be viewed as approximations of the single-particle energies in the deformed Nilsson orbits. As a matter of fact these are very close to the single-particle energies (2.9) of the projected Nilsson model. In order to compare the two models one must first relate the nuclear deformation with deformation parameter d defining the coherent state (3.6). By equating the leading deformation terms of both expressions for the single-particle energies, one arrives at the relation:

$$\frac{d}{k} = \sqrt{\frac{2\pi}{45}}\left(\Omega_\perp^2 - \Omega_z^2\right), \tag{3.21}$$

where $\Omega_\perp$ and Ω_z can be expressed either in δ or β nuclear deformations. The dependence of the above ratio on the nuclear deformation β is shown in Fig. 2, where it is also compared with the linear correspondence (3.10). It is worth mentioning that the linear dependence is a fairly good approximation even for large values of β. Another interesting feature seen in Fig. 2 is that the relation (3.21) is not symmetric when the sign of β is changed. Indeed, for higher values of β the deviation from linearity is bigger for negative values.

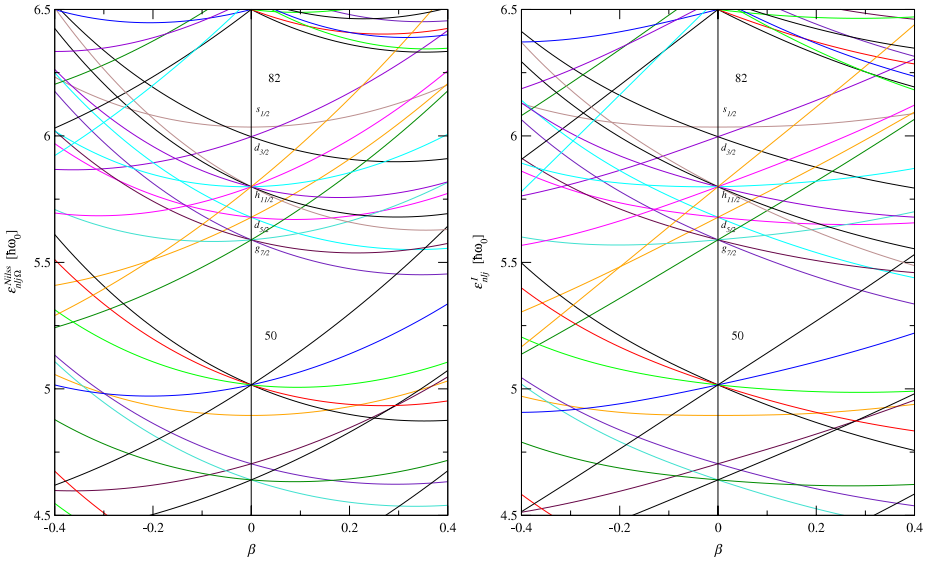

Fig. 3. The proton single-particle energies (2.9) of the projected Nilsson model (left) are compared with those provided by Eq. (3.22) with $k = 10$ (right). The shell model parameters are the same as in Fig. 1.

In virtue of the correspondence (3.21), one can rewrite now the single-particle energies (3.20) as a function of the nuclear deformation as

$$\begin{aligned}\varepsilon^{I}_{nlj}(\beta;k) &= \varepsilon_{nlj} - \hbar\omega_0\left(N+\frac{3}{2}\right)C^{j2j}_{I0I}C^{j2j}_{\frac{1}{2}0\frac{1}{2}}\frac{\left(\Omega_\perp^2-\Omega_z^2\right)}{3}\\ &+\hbar\omega_0\left(N+\frac{3}{2}\right)\left[1+\frac{\sum_J\left(C^{jIJ}_{I-I0}\right)^2 I^{(1)}_J}{\sum_J\left(C^{jIJ}_{I-I0}\right)^2 I^{(0)}_J}\right]\frac{\left(\Omega_\perp^2-\Omega_z^2\right)^2}{90}\\ &-\hbar\omega_0\left(N+\frac{3}{2}\right)\left[j-I+\frac{1}{2}\left(1-(-)^{j-I}\right)\right]\frac{1}{8\pi k^2}.\end{aligned} \tag{3.22}$$

These energies can be directly compared to those obtained in the framework of the projected Nilsson model, due to the dependence on the same deformation variable. This is done in Fig. 3 for protons and Fig. 4 for neutrons. The similarity between the two model single-particle energies is obvious. There are of course some differences, mainly in the large deformation regime. The projected Nilsson model energies are more bent than the energies provided by Eq. (3.22). In the dependence on the deformation parameter d of the latter, the canonical transformation constant k was responsible for the degree of the lines' bending. However, the energy dependence on the nuclear deformation β, as given in (3.22), is almost insensible to the variation of k. It is worth mentioning that for a chosen nucleus and a given value of β, the last occupied single-particle states in the two models differ from each other due to the small displacement of the level crossing. This is an important difference between the two approaches, given the fact that the valence nucleons play an important role in many phenomena.

Concluding, the projected spherical single particle and projected Nilsson model bases provide similar single particle energies. Small differences are noticed for very large deformations where the Nilsson model energy curves are more bent. Also, in that region of deformation some differences in the level crossings may occur. This in turn generates differences in filling up the last occupied states which might be important for those properties determined mainly by the valence nucleons.

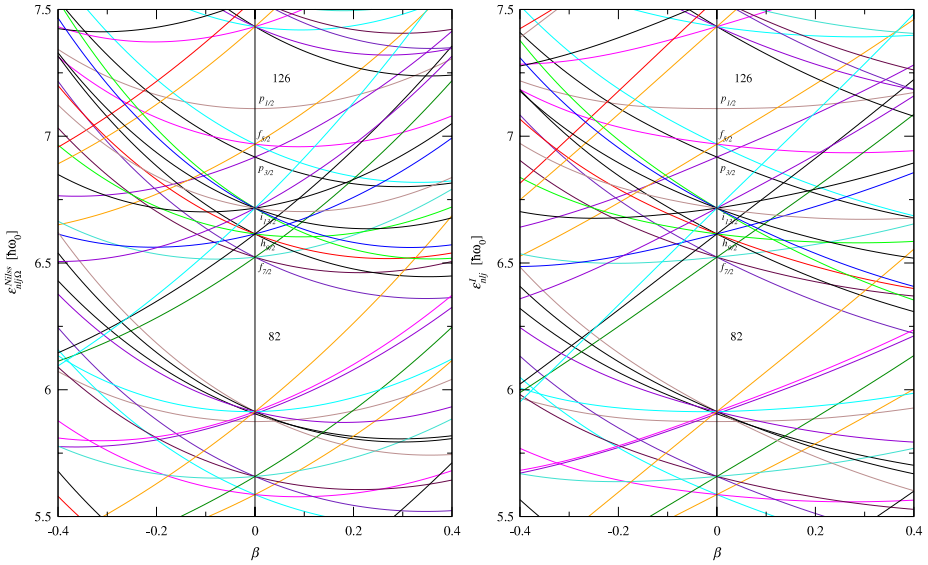

Fig. 4. The neutron single-particle energies (2.9) of the projected Nilsson model (left) are compared with those provided by Eq. (3.22) with $k = 10$ (right). The shell model parameters are the same as in Fig. 1.

3.2. Nucleon density function

Another property of the spherical projected single-particle basis is the distribution of the nucleons on the states associated to the energies (3.20). In the previous subsection one showed the similarity of these single-particle energies with those of the projected Nilsson model. However, the quantum numbers indexing the states are different in the two cases. From the comparison of the two schemes it is obvious that the projection I of the spherical projected single-particle basis (3.12) plays the role of the Ω quantum number from the Nilsson model, and moreover have the same domain of values. Besides the double degeneracy coming from the K and $-K$ invariances, common to both sets of quantum numbers, the states of basis (3.12) are also $2I + 1$ degenerate with respect to M. Since the quantum number I is similar to Ω in the Nilsson model, the number of nucleons having the same I must be at most 2. To fulfill this restriction, the function normalization should be changed to:

$$\|\Phi^{IM}_{nlj}\|^2 = 1 \rightarrow \sum_{M} \|\Phi^{IM}_{nlj}\|^2 = 2.$$

Because the matrix elements of the particle-like operators depend only on the intrinsic quantum number I, the mentioned normalization amounts to introduce an occupation-number probability of $2/(2I + 1)$ for each state Φ^{IM}_{nlj}. In particular, the density operator corresponding to the projected spherical states can be written as:

$$\hat{\rho} = \sum_{nljIM} \frac{2}{2I+1} \left|\Phi^{IM}_{nlj}(d)\right|^2 . \tag{3.23}$$

Using the tensorial form of the projected particle–core state (3.13), and replacing the product of the projected core states and their corresponding complex conjugates by their scalar product, one obtains:

$$\langle\hat{\rho}\rangle_{coll} = 2 \sum_{nljm>0} |||nljm\rangle|^2 , \tag{3.24}$$

which is exactly the spherical shell model nucleon density. The consistency with the projected Nilsson states is then complete.

Thus, although the projected spherical state carries the nuclear deformation through the projected core states, the rotational symmetry, reclaimed by the projected spherical operation, prevails in what the nuclear density function is concerned.

However, it is desirable to induce a deformation dependence of the particles distribution. Inspired by the fact that the deformation dependence of the mean field is obtained by averaging the particle–core Hamiltonian with the quadrupole boson coherent state (3.6), we extend the procedure to the nucleon density (3.23) with the results:

$$\langle\psi_g|\hat{\rho}|\psi_g\rangle = \sum_{nljIM} \frac{2}{2I+1} \left|\langle\psi_g|\Phi^{IM}_{nlj}(d)\rangle\right|^2. \tag{3.25}$$

Similarly, the wave function associated to the deformed single particle mean field might be viewed as the overlap of the projected spherical state with the core's coherent state:

$$\langle\psi_g|\Phi^{IM}_{nlj}(d)\rangle = \mathcal{N}^I_j \sum_J F^{jI}_{JM}(d)|nljM\rangle, \tag{3.26}$$

where

$$F^{jI}_{JM}(d) = C^{jJI}_{I\,0\,I} C^{jJI}_{M\,0\,M} \left(N^{(c)}_J\right)^{-2}. \tag{3.27}$$

At this point it is worth comparing the deformation effect provided by (3.25) with that calculated with the unprojected Nilsson states:

$$\rho^{Nilss} = \sum_{N\Omega\alpha} ||N\Omega\alpha\rangle|^2 = \sum_{\substack{N\Omega\alpha \\ jj'}} C^{\alpha}_{j}(\delta) \left(C^{\alpha}_{j'}(\delta)\right)^* |Nlj\Omega\rangle\langle Nlj'\Omega|. \tag{3.28}$$

Although the deformation is accounted for in different manners by the two approaches, one expects however some similarities.

A direct connection between the k-pole transition densities defined by the projected spherical single particle and the spherical shell model bases, can be obtained by using the second quantization form of a one body operator, which is a tensor of rank k and projection m with respect to the rotation transformations[2]:

$$\begin{aligned}
\hat{T}_{km} &= \sum \sqrt{\frac{2}{2I+1}} \langle\Phi^{IM}_{nlj}|\hat{T}_{km}|\Phi^{I'M'}_{n'l'j'}\rangle \sqrt{\frac{2}{2I'+1}} c^{\dagger}_{\alpha IM} c_{\alpha' I' M'} \\
&= \sum \frac{2}{\hat{I}\hat{I}'} \langle\Phi^{I}_{nlj}\|\hat{T}_k\|\Phi^{I'}_{n'l'j'}\rangle C^{I'kI}_{M'mM} c^{\dagger}_{\alpha IM} c_{\alpha' I' M'} \\
&= \sum_{\alpha I;\alpha' I'} \frac{2}{\hat{I}\hat{I}'} \langle\alpha I\|\hat{T}_k\|\alpha' I'\rangle \hat{\rho}^{ps}_{km}(\alpha I;\alpha' I').
\end{aligned} \tag{3.29}$$

For the sake of simplicity we have used the abbreviations and notations:

$$\begin{aligned}
&|\alpha IM\rangle = |\Phi^{IM}_{nlj}\rangle, \qquad \alpha = (nlj), \qquad \hat{I} = \sqrt{2I+1}, \\
&\hat{\rho}^{ps}_{km}(\alpha I;\alpha' I') = -\frac{\hat{I}}{\hat{k}} \left(c^{\dagger}_{\alpha I} c_{\widetilde{\alpha' I'}}\right)_{km}, \qquad c_{\widetilde{\alpha IM}} = (-1)^{I-M} c_{\alpha I,-M}.
\end{aligned} \tag{3.30}$$

The upper index "ps" accompanying the density matrix indicate that it is associated to the "projected spherical" single particle basis. Changing the single particle basis to that of spherical shell model and

[2] Throughout this paper Rose's convention [41] for the reduced matrix elements is used.

following the same procedure one finds:

$$\hat{T}_{km} = \sum \langle nlj\|\hat{T}_k\|n'l'j'\rangle \hat{\rho}^{sm}_{km}(nlj;\, n'l'j'), \quad \text{with}$$

$$\hat{\rho}^{sm}_{km}(nlj;\, n'l'j') = -\frac{\hat{j}}{\hat{k}}\left(c^{\dagger}_{nlj}\tilde{c}_{n'l'j'}\right)_{km}. \tag{3.31}$$

The connection of the reduced matrix elements in the two bases, projected spherical and spherical shell models, was established in Ref. [39]:

$$\langle \Phi^{I}_{nlj}\|\hat{T}_k\|\Phi^{I'}_{n'l'j'}\rangle = f^{j'I'}_{jI;k}(d)\langle nlj\|\hat{T}_k\|n'l'j'\rangle,$$

$$f^{j'I'}_{jI;k}(d) = \mathcal{N}^{I}_{j}\mathcal{N}^{I'}_{j'}\hat{j}\hat{I}'\sum_{J} C^{j\,J\,I}_{I\,0\,I}C^{j'\,J\,I'}_{I'\,0\,I'}W(jkJI';j'I)\left(N^{c}_{J}\right)^{-2}. \tag{3.32}$$

Using this equation and the linear independence of the nucleon transition densities for different pairs of shell model states one obtains:

$$\hat{\rho}^{sm}_{km}(nlj;\, n'l'j') = \sum_{I,I'}\frac{2}{\hat{I}\hat{I}'}f^{j'I'}_{jI;k(d)}\hat{\rho}^{ps}_{km}(nljI;\, n'l'j'I'). \tag{3.33}$$

Taking into account the explicit expression of the norms $\mathcal{N}^{I}_{j}$ and the analytical form of the Racah coefficient with one vanishing index, it can be proved that for $k = 0$ the factor f is equal to unity:

$$f^{j'I'}_{jI;0}(d) = \delta_{I,I'}\delta_{j,j'}. \tag{3.34}$$

Consequently, we have:

$$\hat{\rho}^{sm}_{00}(nlj;\, nlj) = \sum_{I}\frac{2}{2I+1}\hat{\rho}^{ps}_{00}(nljI;\, nljI). \tag{3.35}$$

Going back to the definition of $\hat{\rho}$ in the two bases, (3.30) and (3.31), by a direct and simple calculation one finds that Eqs. (3.24) and (3.35) are identical.

4. Deformed single-particle and collective motions

To study the particle–core interaction of the whole nucleus one has to consider separate cores and single-particle orbits for protons and neutrons. To this purpose, the CSM has been extended [21,22,42] by assuming that the collective excitations of the proton and neutron systems are independent and therefore described by distinct boson operators, $b^{\dagger}_{p\mu}$ and $b^{\dagger}_{n\mu}$. The extended version is conventionally called the generalized coherent state model (GCSM). In the framework of GCSM the phenomenological core is described by a coherent state of the form (3.6) with the inclusion of the isospin degrees of freedom:

$$\psi^{GCSM}_{g} = e^{d_n\left(b^{\dagger}_{n0}-b_{n0}\right)}e^{d_p\left(b^{\dagger}_{p0}-b_{p0}\right)}|0\rangle_p|0\rangle_n, \tag{4.1}$$

where one considered different deformations for the proton and neutron systems, d_p and d_n. The ground band state is defined as in CSM, through the angular momentum projection of the above coherent state. The norm of the projected state

$$\phi^{g}_{JM}(d_n, d_p) = N_J(d_p, d_n)P^{J}_{M0}\psi^{GCSM}_{g} \tag{4.2}$$

and the corresponding matrix elements of the boson invariants can also be expressed in terms of the overlap integrals (3.16), if one replaces "d" with "ρ" defined by

$$\rho^2 = d_n^2 + d_p^2. \tag{4.3}$$

Similarly, if one considers for the description of the phenomenological collective core a quadrupole harmonic boson Hamiltonian,

$$H_{core}^{GCSM} = \omega_b \sum_{\tau\mu} b_{\tau\mu}^{\dagger} b_{\tau\mu}, \tag{4.4}$$

then the ground band energies are also functions of the global deformation parameter ρ alone,

$$\begin{aligned} E_J(\rho) &= \langle \phi_{JM}^g(d_n, d_p) | H_{core}^{GCSM} | \phi_{JM}^g(d_n, d_p) \rangle \\ &= \omega_b \rho^2 \frac{I_J^{(1)}(\rho^2)}{I_J^{(0)}(\rho^2)}. \end{aligned} \tag{4.5}$$

Although the projected wave function depends on two independent deformation parameters, d_p and d_n, the ground band energy depends only on ρ. Using this expression for the energy of the first two excited states, one can easily find ρ for any nucleus by fitting the calculated ratio

$$R_{4/2} = \frac{E_{4^+}(\rho) - E_{0^+}(\rho)}{E_{2^+}(\rho) - E_{0^+}(\rho)} \tag{4.6}$$

to the corresponding experimental value. Even if the ground band energies depend only on ρ, this is not a suitable deformation variable since there are observables, which depend explicitly on both d_p and d_n. If one considers $d = d_n = d_p$ then the single-particle and collective features of the nuclear structure can be described through a single isospin independent deformation parameter d and a unique canonical transformation constant k. ρ can be extracted from experiment, as explained above, and then through the relation $\rho = \sqrt{2}d$, one gets d, while k can be fixed by using Eq. (3.21) for a known nuclear deformation β. Of course this is an oversimplified case because in general the deformation features of the proton and neutron subsystems are different even if not very much. In order to determine the isospin differentiated deformation parameters d_p and d_n one must fit besides the ratio (4.6) another observable which must be isospin dependent. Such a quantity is $B(E2)$ transition probability which is dominantly determined by the proton degrees of freedom. The $E2$ transition operator is given as [43]:

$$T_{2\mu} = \frac{3Ze}{4\pi} R_0^2 \alpha_{p\mu}, \tag{4.7}$$

where $\alpha_{p\mu}$ is the proton quadrupole shape variable defined in terms of proton boson operators as in Eq. (3.3) R_0 denotes the nuclear radius. The reduced matrix element of $\alpha_{p\mu}$ between the GCSM projected ground states is expressed as [22]

$$\langle \phi_J^g(d_n, d_p) \| \alpha_p \| \phi_{J'}^g(d_n, d_p) \rangle = \frac{1}{2k_p} C_{0\,0\,0}^{J'\,2\,J} \rho \frac{N_J}{N_{J'}} \left[1 + \frac{2J'+1}{2J+1} \left(\frac{N_{J'}}{N_J} \right)^2 \right]. \tag{4.8}$$

In the Bohr–Mottelson parameterization [38], the rotational invariance of the nuclear potential leads to $\sum_\mu \alpha_{2\mu} \alpha_{2\mu}^* = \beta^2$, such that the $E2$ transition probability between $J = 0$ and $J = 2$ ground states can be written as

$$\begin{aligned} B(E2; 0^+ \to 2^+) &= \left| \langle \phi_0^g(d_n, d_p) \| T_{2\mu} \| \phi_2^g(d_n, d_p) \rangle \right|^2 \\ &= \left(\frac{3}{4\pi} \right)^2 e^2 Z^2 R_0^4 \beta^2. \end{aligned} \tag{4.9}$$

Using Eq. (4.8) in the above equation one obtains [43]:

$$\beta = \frac{\sqrt{5}}{2} \frac{\rho}{k_p} \left[\frac{N_2}{N_0} + \frac{1}{5} \frac{N_0}{N_2} \right], \tag{4.10}$$

which relates the nuclear deformation β with the global deformation parameter ρ and the proton canonical transformation constant k_p. The global deformation parameter ρ being fixed by fitting the

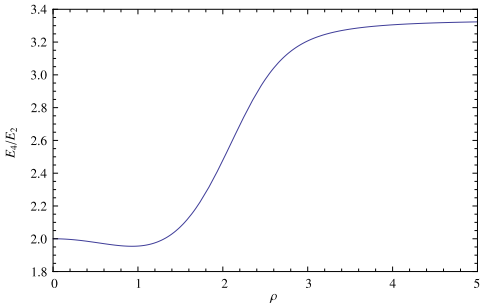

Fig. 5. The theoretical ratio $R_{4/2}$ given by Eq. (4.6) as a function of the global deformation parameter ρ. The mentioned ratio reaches the absolute minimum at $\rho = 0.930$. The minimum value is 1.954.

experimental value of $R_{4/2}$ and with nuclear deformation β taken from nuclear data tables, the above expression becomes a determining equation for k_p. Making use of Eqs. (3.21) and (4.3) alternatively for protons and neutrons, one determines the complete set of parameters d_p, d_n, k_p and k_n which are needed for a consistent description of the collective and single-particle degrees of freedom.

5. Numerical application and discussions

For a complete understanding of the formalism based on the spherical projected single-particle basis, it would be useful to determine the domain of values for the deformation parameters d, d_p and d_n as well as of the corresponding canonical transformation constants k, k_p and k_p. We chose to make such a systematics for isotopic chains of medium and heavy nuclei whose occupied single-particle states cover $N = 4$ and $N = 5$ proton shells but not fill them completely. Thus, one performed calculations for the isotopic chains of Ge, Se, Zr, Mo, Cd, Te, Sm, Gd, Dy, Er, Hf, Os, Pt, Th and U. In order to obtain the parameters describing each nucleus, one first determines its global parameter ρ by fitting the experimental value of the ratio $R_{4/2}$ with the theoretical expression (4.6). Before doing this for all considered isotopes, it is instructive to investigate the behavior of the theoretical ratio $R_{4/2}$ as a function of the global deformation parameter ρ, defined by Eq. (4.6). Using the asymptotic [44] and vibrational limits [45] of the overlap integrals (3.16), one can easily check that for $\rho \to \infty$ one have $R_{4/2} = 3.33$ which is exactly the value provided by the axially symmetric rotor model, while for $\rho \to 0$ one obtains the spherical vibrator value $R_{4/2} = 2$. What happens between these two limiting cases can be seen in Fig. 5, where the expression (4.6) of $R_{4/2}$ is plotted as a function of ρ. From there one notices that the function (4.6) acquires even values smaller than two. Moreover, it exhibits a minimum value of 1.954 reached at $\rho = 0.930$, such that there exists an interval where for two distinct ρ the ratio takes a common value. The ambiguity of $R_{4/2}$ is removed by restricting our considerations to the values $\rho \geq 0.930$ where the function has a bijective character. Another fact which is worth to be mentioned, is that starting from relatively small values of $\rho(\approx 3.6)$ the ratio $R_{4/2}$ approaches asymptotically the rotational value $R_{4/2} = 3.33$. These findings allow us to define the domain of accepted values for the global deformation parameter ρ, to be $0.930 < \rho < 5$.

Note that the global deformation parameter can be fixed in the way described above only for nuclei for which energies of the first two collective excited states are known. After fixing it one can further get an isospin independent deformation parameter $d = \rho/\sqrt{2}$ which describes the single-particle aspects of the corresponding nucleus. Using this value in Eq. (3.21) together with a tabulated nuclear deformation [46] one obtains the canonical transformation constant k valid for both proton and neutron single-particle degrees of freedom. In order to obtain isospin differentiated deformation parameters d_p and d_n with corresponding scaling constants k_p and k_n, one first make use of Eq. (4.10) where one plugs the value of ρ obtained before as well as the nuclear deformation taken from Ref. [46] to obtain k_p. The rest of the parameters are easily obtained by considering the relation (3.21) for protons and neutrons taking also into account the relation (4.3) between the deformation parameters. All of these quantities are listed in Tables 1–15 for each considered isotopic chain where

Table 1
Numerical values of ρ, d, k, d_p, k_p, d_n and k_n obtained for the isotopic chain of Ge($Z = 32$). The nuclear deformation β taken from [46] and the experimental value of $R_{4/2}$ taken from [50], are also listed. For nuclei with $R_{4/2} < 1.7$ the calculations were not possible. For ^{74}Ge we replaced β_2 from Ref. [46] with the corresponding experimental value [51]. In this way one removes the inconsistency with the sign of the quadrupole moment for the state 2^+.

Nucleus	N	β	$R_{4/2}$	ρ	d	k	d_p	k_p	d_n	k_n
^{64}Ge	32	0.219	2.276	1.794	1.269	8.6855	1.228	8.4070	1.308	8.9554
^{66}Ge	34	0.229	2.271	1.788	1.264	8.2965	1.222	8.0168	1.306	8.5671
^{68}Ge	36	−0.275	2.233	−1.742	−1.232	5.7072	−1.409	6.5295	−1.024	4.7444
^{70}Ge	38	−0.241	2.071	−1.497	−1.059	5.6803	−1.234	6.6225	−0.847	4.5468
^{74}Ge	42	0.290*	2.457	1.979	1.399	7.3412	1.321	6.9291	1.474	7.7315
^{76}Ge	44	0.143	2.505	2.025	1.432	14.7473	1.394	14.3528	1.469	15.1316
^{78}Ge	46	0.153	2.535	2.053	1.452	14.0091	1.408	13.5871	1.494	14.4187
^{80}Ge	48	0.144	2.644	2.153	1.522	15.5746	1.476	15.0968	1.568	16.0381
^{82}Ge	50	0.053	1.505							
^{84}Ge	52	0.142	2.676	2.183	1.544	16.0059	1.496	15.5121	1.590	16.4849

Table 2
The same as in Table 1 but for the isotopic chain of Se($Z = 34$). Here for nucleus ^{72}Se, the experimental ratio $R_{4/2}$ is not much smaller than the minimum theoretical value 1.954 and one can adopt the corresponding minimum value. However, the yielded value $\rho = 0.930$ would further produce $d_p > \rho$, which contradicts Eq. (4.3). Due to this reason for this nucleus one takes that ρ which corresponds to the tabulated β value and lies on the line obtained by fitting the rest of the points for this isotopic chain (Fig. 6). Also, for ^{74,76}Se we replaced β_2 from Ref. [46] with the corresponding experimental value [52,53]. In this way one removes the inconsistency with the sign of the quadrupole moment for the state 2^+.

Nucleus	N	β	$R_{4/2}$	ρ	d	k	d_p	k_p	d_n	k_n
^{68}Se	34	0.240	2.275	1.792	1.267	7.9526	1.221	7.6640	1.311	8.2310
^{70}Se	36	−0.307	2.158	−1.643	−1.162	4.7521	−1.363	5.5755	−0.917	3.7523
^{72}Se	38	−0.283	1.899	−2.293	−1.621	7.2735	−1.819	8.1586	−1.396	6.2645
^{74}Se	40	0.240*	2.148	1.628	1.151	7.2248	1.128	7.0805	1.174	7.3662
^{76}Se	42	0.280*	2.380	1.904	1.346	7.3013	1.278	6.9292	1.412	7.6553
^{78}Se	44	0.143	2.449	1.971	1.394	14.3541	1.359	13.9999	1.427	14.6998
^{80}Se	46	0.153	2.554	2.070	1.464	14.1251	1.419	13.6921	1.507	14.5452
^{82}Se	48	0.154	2.650	2.159	1.527	14.6404	1.476	14.1538	1.576	15.1112
^{84}Se	50	0.053	1.459							
^{86}Se	52	0.125	2.227	1.735	1.227	14.3883	1.221	14.3163	1.233	14.4599

one also presented the nuclear deformation taken from [46] and the experimental value of the ratio $R_{4/2}$. The calculated values for the deformation parameter d are in agreement with those obtained for some selected nuclei in Refs. [47–49] where the same parameter was determined by fitting all experimentally available collective states including β and γ rotational states with a more complex quadrupole boson Hamiltonian.

Although the calculations are straightforward for most of the considered nuclei, there are also some special situations where a roundabout method is required to obtain consistent results. As can be seen from Tables 1–15, the nuclei around a shell closure always exhibit a ratio $R_{4/2}$ smaller than two and sometimes even smaller than the theoretical minimum value predicted by Eq. (4.6), i.e. 1.954. In these cases one cannot determine the global parameter ρ and consequently any other quantity of interest. However, in some cases even if $R_{4/2} < 1.954$ but not much smaller, one can still consider the value $\rho = 0.930$ corresponding to the minimum of Eq. (4.6). This approximation was made for nuclei with $1.7 < R_{4/2} < 1.954$ which are indicated in the captions of Tables 4–11 and 14. Another difficulty arises when computing the deformation parameters and canonical transformation constants for vanishing or very small values of the nuclear deformation β. Indeed, the calculation algorithm explained above cannot be applied in the case of vanishing β, while for very small values of β the results for the canonical constants are too large to be taken into account. In order to avoid this problem and therewith to obtain a description of these nuclei, one uses different values for the nuclear deformation β found by interpolating the linear fit of the remaining (ρ, β) data points for a certain isotopic chain. In Tables 1–15 the interpolated values are replacing those taken from Ref. [46] and the

Table 3
Same as in Table 1 but for the isotopic chain of Zr($Z = 40$). For few nuclei, ^{82,84,86,88}Zr, the nuclear deformation β is too small to provide acceptable results. For these nuclei one considered the nuclear deformation β^{fit} corresponding to the linear fit from Fig. 6 performed for the rest of the data points.

Nucleus	N	β	β^{fit}	$R_{4/2}$	ρ	d	k	d_p	k_p	d_n	k_n
^{80}Zr	40	0.433		2.858	2.365	1.672	6.0102	1.529	5.4944	1.804	6.4850
^{82}Zr	42	0.053	0.299	2.557	2.073	1.466	7.4710	1.377	7.0158	1.550	7.9001
^{84}Zr	44	0.053	0.269	2.339	1.862	1.317	7.4162	1.255	7.0705	1.375	7.7465
^{86}Zr	46	0.053	0.249	2.217	1.723	1.218	7.3838	1.179	7.1454	1.256	7.6149
^{88}Zr	48	0.053	0.200	2.024	1.386	0.980	7.3165	1.015	7.5793	0.944	7.0439
^{90}Zr	50	0.053		1.407							
^{92}Zr	52	0.053		1.600							
^{94}Zr	54	0.062		1.600							
^{96}Zr	56	0.217		1.571							
^{98}Zr	58	0.330		1.674							
^{100}Zr	60	0.358		2.656	2.165	1.531	6.5834	1.420	6.1046	1.635	7.0296
^{102}Zr	62	0.369		3.151	2.819	1.993	8.3309	1.833	7.6590	2.142	8.9526
^{104}Zr	64	0.381		3.246	3.197	2.261	9.1672	2.072	8.4032	2.434	9.8723
^{106}Zr	66	0.373		3.133	2.774	1.962	8.1150	1.803	7.4574	2.109	8.7233
^{108}Zr	68	0.365		3.003	2.542	1.797	7.5899	1.656	6.9933	1.928	8.1429

Table 4
Same as in Table 1 but for the isotopic chain of Mo($Z = 42$). For few nuclei, ^{84,86,88,90,94,96}Mo, the nuclear deformation β is too small to provide acceptable results. For these nuclei one considered the nuclear deformation β^{fit} corresponding to the linear fit from Fig. 6 performed for the rest of the data points. The experimental ratio $R_{4/2}$ for ^{94}Mo and ^{98}Mo is not much smaller than the minimum theoretical value 1.954 such that one adopted for them the corresponding minimum value $\rho = 0.930$.

Nucleus	N	β	β^{fit}	$R_{4/2}$	ρ	d	k	d_p	k_p	d_n	k_n
^{84}Mo	42	0.053	0.299	2.517	2.036	1.440	7.3377	1.354	6.8990	1.521	7.7516
^{86}Mo	44	0.053	0.274	2.343	1.866	1.319	7.3037	1.256	6.9547	1.380	7.6368
^{88}Mo	46	0.053	0.256	2.235	1.745	1.234	7.2841	1.190	7.0242	1.276	7.5350
^{90}Mo	48	0.053	0.231	2.112	1.571	1.111	7.2296	1.100	7.1572	1.122	7.3013
^{92}Mo	50	0.035		1.512							
^{94}Mo	52	0.053	0.137	1.807	0.930	0.658	7.0587	0.864	9.2779	0.343	3.6839
^{96}Mo	54	0.080	0.226	2.092	1.536	1.086	7.2171	1.083	7.1940	1.090	7.2402
^{98}Mo	56	0.180		1.918	0.930	0.658	5.4296	0.855	7.0615	0.365	3.0158
^{100}Mo	58	0.244		2.121	1.587	1.122	6.9332	1.105	6.8281	1.139	7.0367
^{102}Mo	60	0.329		2.507	2.027	1.433	6.6748	1.341	6.2442	1.520	7.0794
^{104}Mo	62	0.349		2.917	2.431	1.719	7.5718	1.590	7.0017	1.839	8.1020
^{106}Mo	64	0.361		3.045	2.605	1.842	7.8593	1.698	7.2427	1.976	8.4309
^{108}Mo	66	0.333		2.924	2.439	1.725	7.9405	1.599	7.3616	1.842	8.4800
^{110}Mo	68	0.335		2.805	2.309	1.633	7.4749	1.516	6.9389	1.742	7.9750

corresponding nuclei are indicated in captions or are simply given in a separate column for isotopic chains with more such cases. The linear fits used for interpolation are shown in Figs. 6 and 7 for the lighter and heavier isotopic chains respectively, where the equation of the fitting line is indicated for each one of them. It must be mentioned that due to the relation between β and d the linear fits are restricted to have a vanishing intercept. The same fits are also used for interpolating values of ρ for nuclei where this cannot be determined (^{240}U) or where the value obtained in the usual way provides results conflicting the relation (4.3) (^{72}Se). The sign of the nuclear deformation β is carried towards the deformation parameters d, d_p and d_n, but in the case of the vanishing β one choose by default the positive values for the deformation parameters d, d_p and d_n.

The slope of the fits can be viewed as an average value of the k over the chosen isotopic chain. As a matter of fact this result is consistent with the linear dependence (3.10) of d/k on the nuclear deformation β given the fact that $\rho = \sqrt{2}d$.

A natural question concerning the consistency of the fitted deformation parameters with the experimental quadrupole moment for the collective state 2^+, Q_2^{Exp}, arises. According to Ref. [54] for

Table 5
The same as in Table 1 but for the isotopic chain of Cd($Z = 48$). For few nuclei, ^{100,102,104,124,126,128}Cd, the nuclear deformation β is zero or too small to provide acceptable results. For these nuclei one considered the nuclear deformation β^{fit} corresponding to the linear fit from Fig. 6 performed for the rest of the data points. The experimental ratio $R_{4/2}$ for ^{100}Cd is not much smaller than the minimum theoretical value 1.954 such that one adopted for it the corresponding minimum value $\rho = 0.930$. For two isotopes ^{98,130}Cd the algorithm of this paper fails since the ratio $R_{4/2}$ is too small.

Nucleus	N	β	β^{fit}	$R_{4/2}$	ρ	d	k	d_p	k_p	d_n	k_n
^{98}Cd	50	0.027		1.493							
^{100}Cd	52	0.035	0.079	1.792	0.930	0.658	12.0608	0.878	16.1011	0.307	5.6288
^{102}Cd	54	0.053	0.133	2.109	1.567	1.108	12.2373	1.123	12.4056	1.093	12.0667
^{104}Cd	56	0.089	0.151	2.268	1.784	1.261	12.2945	1.241	12.0996	1.281	12.4863
^{106}Cd	58	0.126		2.361	1.885	1.333	15.5122	1.311	15.2606	1.354	15.7598
^{108}Cd	60	0.135		2.383	1.907	1.348	14.6811	1.322	14.3920	1.374	14.9646
^{110}Cd	62	0.144		2.345	1.868	1.321	13.5129	1.295	13.2458	1.346	13.7748
^{112}Cd	64	0.144		2.292	1.812	1.281	13.1078	1.261	12.8966	1.302	13.3157
^{114}Cd	66	0.163		2.299	1.819	1.286	11.6795	1.259	11.4316	1.313	11.9224
^{118}Cd	70	−0.241		2.388	−1.912	−1.352	7.2549	−1.506	8.0809	−1.178	6.3219
^{120}Cd	72	0.135		2.379	1.903	1.346	14.6503	1.319	14.3649	1.371	14.9302
^{122}Cd	74	0.108		2.334	1.857	1.313	17.7443	1.300	17.5690	1.326	17.9179
^{124}Cd	76	0.000	0.151	2.260	1.775	1.255	12.2921	1.236	12.1084	1.274	12.4731
^{126}Cd	78	0.000	0.150	2.250	1.763	1.247	12.2890	1.230	12.1205	1.263	12.4552
^{128}Cd	80	0.000	0.146	2.215	1.721	1.217	12.2780	1.206	12.1672	1.228	12.3879
^{130}Cd	82	0.000		1.407							

Table 6
The same as in Table 1 but for the isotopic chain of Te($Z = 52$). For few nuclei, $^{128-138}$Te, the nuclear deformation β is zero such that for these nuclei one considered the nuclear deformation β^{fit} corresponding to the linear fit from Fig. 6 performed for the rest of the data points. The experimental ratio $R_{4/2}$ for ^{130}Te and ^{132}Te is not much smaller than the theoretical minimum value 1.954 hence one adopted for them the corresponding minimum value $\rho = 0.930$. The horizontal line after ^{134}Te indicates the change of neutron shell model parameters κ and μ.

Nucleus	N	β	β^{fit}	$R_{4/2}$	ρ	d	k	d_p	k_p	d_n	k_n
^{106}Te	54	0.099		2.035	1.416	1.001	14.7246	1.056	15.5232	0.944	13.8802
^{108}Te	56	0.134		2.062	1.477	1.044	11.4526	1.076	11.7988	1.012	11.0957
^{110}Te	58	0.152		2.133	1.605	1.135	11.0214	1.139	11.0564	1.131	10.9863
^{112}Te	60	0.161		2.142	1.620	1.146	10.5259	1.144	10.5141	1.147	10.5376
^{114}Te	62	0.161		2.094	1.539	1.088	9.9996	1.101	10.1129	1.076	9.8849
^{116}Te	64	0.180		2.002	1.319	0.933	7.7006	0.990	8.1731	0.872	7.1972
^{118}Te	66	−0.147		1.992	−1.279	−0.904	8.2657	−1.076	9.8359	−0.691	6.3166
^{120}Te	68	−0.156		2.073	−1.499	−1.060	9.0970	−1.193	10.2405	−0.907	7.7873
^{128}Te	76	0.000	0.141	2.014	1.358	0.960	10.0596	1.017	10.6537	0.900	9.4280
^{130}Te	78	0.000	0.096	1.945	0.930	0.658	9.9430	0.874	13.2105	0.319	4.8176
^{132}Te	80	0.000	0.096	1.716	0.930	0.658	9.9430	0.874	13.2105	0.319	4.8176
^{134}Te	82	0.000		1.232							
^{136}Te	84	0.000		1.698							
^{138}Te	86	0.000	0.148	2.040	1.428	1.010	10.0779	1.048	10.4597	0.970	9.6811

50 nuclei considered here, there are experimental data for the quadrupole moment of the lowest 2^+. For 42 of them the signs of $Q_2^{Exp.}$ and β as given in Ref. [46] are consistent with each other, i.e., they are opposite. For three of the remaining eight, the sign prediction of Ref. [46] for β is different from that of the experimental nuclear quadrupole deformation. Choosing β as given by experiment one obtains agreement with the sign of Q_2^{Exp} also for ^{74}Ge and ^{74,76}Se. As for the remaining 5 nuclei we slightly changed the algorithm of fixing the parameters due to the lack of experimental data for the quadrupole deformation.

Table 7
The same as in Table 1 but for the isotopic chain of Sm($Z = 62$). For ^{142}Sm and ^{146}Sm the nuclear deformation β is zero such that for these nuclei one considered and listed the nuclear deformation corresponding to the linear fit from Fig. 7 performed for the rest of the data points. The experimental ratio $R_{4/2}$ for ^{146}Sm is not much smaller than the minimum theoretical value 1.954 hence one adopted for it the corresponding minimum value $\rho = 0.930$. The horizontal line indicates the change of neutron shell model parameters κ and μ.

Nucleus	N	β	$R_{4/2}$	ρ	d	k	d_p	k_p	d_n	k_n
^{132}Sm	70	0.323	3.183	2.913	2.060	9.7604	1.907	9.0383	2.202	10.4327
^{134}Sm	72	0.312	2.939	2.457	1.737	8.5062	1.616	7.9137	1.850	9.0600
^{136}Sm	74	0.237	2.692	2.199	1.555	9.8760	1.474	9.3591	1.632	10.3672
^{138}Sm	76	0.190	2.571	2.086	1.475	11.5647	1.416	11.1056	1.531	12.0062
^{140}Sm	78	−0.148	2.348	−1.871	−1.323	12.0053	−1.422	12.9062	−1.216	11.0310
^{142}Sm	80	0.171	2.332	1.855	1.312	11.3755	1.278	12.9062	1.344	11.6581
^{144}Sm	82	0.000	1.320							
^{146}Sm	84	0.086	1.849	0.930	0.658	11.0931	0.876	14.7800	0.312	5.2597
^{148}Sm	86	0.161	2.145	1.624	1.148	10.5519	1.146	10.5344	1.150	10.5693
^{150}Sm	88	0.206	2.316	1.837	1.299	9.4276	1.257	9.1235	1.340	9.7223
^{152}Sm	90	0.243	3.009	2.551	1.804	11.1882	1.699	10.5408	1.903	11.8001
^{154}Sm	92	0.270	3.255	3.261	2.306	12.9428	2.155	12.0937	2.448	13.7395
^{156}Sm	94	0.279	3.290	3.666	2.592	14.1057	2.417	13.1502	2.757	15.0005
^{158}Sm	96	0.279	3.301	3.880	2.744	14.9291	2.557	13.9155	2.918	15.8782
^{160}Sm	98	0.290	3.291	3.668	2.594	13.6067	2.413	12.6583	2.763	14.4932

Table 8
The same as in Table 1 but for the isotopic chain of Gd($Z = 64$). For ^{144}Gd and ^{148}Gd the nuclear deformation β is zero such that for these nuclei one considered and listed the nuclear deformation corresponding to the linear fit from Fig. 7 performed for the rest of the data points. The experimental ratio $R_{4/2}$ for ^{148}Gd is not much smaller than the minimum theoretical value 1.954 hence one adopted the corresponding minimum value $\rho = 0.930$. The horizontal line indicates the change of neutron shell model parameters κ and μ.

Nucleus	N	β	$R_{4/2}$	ρ	d	k	d_p	k_p	d_n	k_n
^{138}Gd	74	0.256	2.741	2.245	1.587	9.3712	1.497	8.8379	1.673	9.8759
^{140}Gd	76	0.210	2.545	2.062	1.458	10.3901	1.395	9.9397	1.519	10.8219
^{142}Gd	78	−0.156	2.346	−1.869	−1.322	11.3424	−1.425	12.2327	−1.209	10.3760
^{144}Gd	80	0.160	2.348	1.871	1.323	12.2297	1.291	11.9382	1.354	12.5144
^{146}Gd	82	0.000	1.324							
^{148}Gd	84	0.080	1.806	0.930	0.658	11.9051	0.878	15.8885	0.308	5.5696
^{150}Gd	86	0.161	2.019	1.373	0.971	8.9210	1.019	9.3600	0.921	8.4592
^{152}Gd	88	0.207	2.194	1.693	1.197	8.6486	1.173	8.4714	1.221	8.8223
^{154}Gd	90	0.243	3.015	2.559	1.809	11.2232	1.705	10.5732	1.909	11.8376
^{156}Gd	92	0.271	3.239	3.157	2.232	12.4863	2.086	11.6672	2.370	13.2548
^{158}Gd	94	0.271	3.288	3.629	2.566	14.3531	2.396	13.4022	2.726	15.2447
^{160}Gd	96	0.280	3.302	3.913	2.767	15.0052	2.578	13.9834	2.943	15.9618
^{162}Gd	98	0.291	3.302	3.901	2.758	14.4240	2.565	13.4136	2.939	15.3681
^{164}Gd	100	0.301	3.300	3.863	2.732	13.8348	2.536	12.8420	2.914	14.7609

Let us derive the expression of the quadrupole moment within the GCSM. The liquid drop model (LDM) predicts for the quadrupole moment the expression:

$$Q_{2\mu} = \frac{3ZeR_0^2}{4\pi}\left(\alpha_{2\mu} - \frac{10}{\sqrt{70\pi}}(\alpha_2\alpha_2)_{2\mu}\right), \quad R_0 = 1.2A^{1/3}fm. \tag{5.1}$$

Within LDM the state 2^+ is a one phonon state, $b^\dagger_{2\mu}|0\rangle$, which yields for the quadrupole moment, with the standard definition, the expression:

$$\langle 22|Q_{20}|22\rangle = -\frac{3ZeR_0^2\sqrt{5}}{7\pi k^2\sqrt{\pi}}. \tag{5.2}$$

Table 9
The same as in Table 1 but for the isotopic chain of Dy($Z = 66$). For ^{146}Dy and ^{150}Dy the nuclear deformation β is zero such that for these nuclei one considered and listed the nuclear deformation corresponding to the linear fit from Fig. 7, performed for the rest of the data points. Also, the experimental ratio $R_{4/2}$ for ^{150}Dy is not much smaller than the minimum theoretical value 1.954, hence for it one adopted the corresponding minimum value $\rho = 0.930$. The horizontal line indicates the change of neutron shell model parameters κ and μ.

Nucleus	N	β	$R_{4/2}$	ρ	d	k	d_p	k_p	d_n	k_n
^{140}Dy	74	0.267	2.800	2.304	1.629	9.2417	1.532	8.6879	1.721	9.7642
^{142}Dy	76	0.219	2.529	2.047	1.447	9.9104	1.383	9.4665	1.510	10.3353
^{144}Dy	78	−0.164	2.365	−1.889	−1.336	10.8707	−1.443	11.7468	−1.219	9.9175
^{146}Dy	80	0.158	2.355	1.878	1.328	12.4247	1.296	12.1296	1.359	12.7131
^{148}Dy	82	0.000	1.447							
^{150}Dy	84	0.078	1.813	0.930	0.658	12.2035	0.878	16.2959	0.306	5.6831
^{152}Dy	86	0.153	2.055	1.461	1.033	9.9694	1.063	10.2564	1.002	9.6740
^{154}Dy	88	0.207	2.234	1.743	1.232	8.9040	1.201	8.6786	1.263	9.1239
^{156}Dy	90	0.235	2.934	2.451	1.733	11.0968	1.637	10.4816	1.824	11.6795
^{158}Dy	92	0.262	3.206	3.000	2.121	12.2509	1.986	11.4723	2.248	12.9829
^{160}Dy	94	0.272	3.270	3.400	2.404	13.4006	2.245	12.5137	2.553	14.2322
^{162}Dy	96	0.281	3.294	3.723	2.633	14.2286	2.453	13.2589	2.800	15.1362
^{164}Dy	98	0.292	3.301	3.872	2.809	14.6390	2.611	13.6104	2.993	15.6000
^{166}Dy	100	0.293	3.310	4.173	2.951	15.3302	2.743	14.2488	3.145	16.3402
^{168}Dy	102	0.304	3.313	4.278	3.025	15.1782	2.806	14.0782	3.229	16.2038
^{170}Dy	104	0.295	3.264	3.338	2.360	12.1841	2.195	11.3287	2.515	12.9833

Table 10
The same as in Table 1 but for the isotopic chain of Er($Z = 68$). For ^{152}Er the nuclear deformation β is too small to provide acceptable results such that one considered and listed for this nucleus the nuclear deformation corresponding to the linear fit from Fig. 7 performed for the rest of the data points. Also the experimental ratio $R_{4/2}$ for the same nucleus is not much smaller than the minimum theoretical value 1.954 hence for it one adopted the corresponding minimum value $\rho = 0.930$. The horizontal line indicates the change of neutron shell model parameters κ and μ.

Nucleus	N	β	$R_{4/2}$	ρ	d	k	d_p	k_p	d_n	k_n
^{148}Er	80	−0.156	2.357	−1.881	−1.330	11.4153	−1.433	12.3026	−1.218	10.4529
^{150}Er	82	−0.008	1.453							
^{152}Er	84	−0.074	1.832	−0.930	−0.658	12.2625	−0.921	17.1767	−0.128	2.3870
^{154}Er	86	0.143	2.072	1.499	1.060	10.9167	1.085	11.1715	1.035	10.6558
^{156}Er	88	0.189	2.314	1.836	1.298	10.2302	1.261	9.9394	1.334	10.5128
^{158}Er	90	0.216	2.744	2.248	1.590	11.0274	1.512	10.4879	1.664	11.5417
^{160}Er	92	0.253	3.099	2.702	1.911	11.4056	1.795	10.7129	2.020	12.0586
^{162}Er	94	0.272	3.230	3.107	2.197	12.2457	2.053	11.4415	2.332	13.0004
^{164}Er	96	0.273	3.277	3.471	2.454	13.6330	2.291	12.7270	2.607	14.4823
^{166}Er	98	0.283	3.289	3.636	2.571	13.8032	2.395	12.8586	2.736	14.6872
^{168}Er	100	0.294	3.309	4.131	2.921	15.1271	2.715	14.0577	3.114	16.1258
^{170}Er	102	0.296	3.310	4.153	2.937	15.1106	2.728	14.0369	3.131	16.1129
^{172}Er	104	0.287	3.312	4.228	2.990	15.8390	2.782	14.7381	3.184	16.8682

From here it results that for spherical nuclei the quadrupole moment is always negative. The GCSM defines the state 2^+ by the angular momentum projected state $\phi^g_{JM}(d_n, d_p)$ (see Eq. (4.2)) while the quadrupole moment, in the boson representation, is:

$$Q_{20} = \frac{3ZeR_0^2}{4\pi}\left[\frac{1}{k_p\sqrt{2}}\left(b^\dagger_{b0} + b_{p0}\right) - \frac{5}{k_p^2\sqrt{70\pi}}\left((b^\dagger_p b^\dagger_p)_{20} + (b_p b_p)_{20} + (b^\dagger_p b_p)_{20}\right)\right]. \tag{5.3}$$

Averaging this operator with the projected state mentioned above one obtains:

$$\langle\phi^g_{22}(d_n, d_p)|Q_{20}|\phi^g_{22}(d_n, d_p)\rangle = -\frac{3ZeR_0^2}{7\pi}\left[\frac{1}{\sqrt{2}}\frac{d_p}{k_p} + \frac{1}{7}\sqrt{\frac{5}{\pi}}\left(\frac{d_p}{k_p}\right)^2\left(1 + \frac{I^{(1)}_2(\rho)}{I^{(0)}_2(\rho)}\right)\right]. \tag{5.4}$$

Table 11
The same as in Table 1 but for the isotopic chain of Hf($Z = 72$). For ^{156}Hf the nuclear deformation β is too small to provide acceptable results such that one considered and listed for this nucleus the nuclear deformation corresponding to the linear fit from Fig. 7 performed for the rest of the data points. Also the experimental ratio $R_{4/2}$ for the same nucleus is not much smaller than the minimum theoretical value 1.954 hence for it one adopted the corresponding minimum value $\rho = 0.930$.

Nucleus	N	β	$R_{4/2}$	ρ	d	k	d_p	k_p	d_n	k_n
^{156}Hf	84	0.076	1.849	0.930	0.658	12.5176	0.879	16.7247	0.305	5.8023
^{158}Hf	86	0.107	2.169	1.659	1.173	15.9962	1.182	16.1212	1.164	15.8702
^{160}Hf	88	0.152	2.306	1.827	1.292	12.5458	1.267	12.3059	1.316	12.7813
^{162}Hf	90	0.180	2.560	2.076	1.468	12.1202	1.413	11.6699	1.521	12.5543
^{164}Hf	92	0.208	2.786	2.290	1.619	11.6447	1.542	11.0870	1.693	12.1770
^{166}Hf	94	0.226	2.966	2.491	1.761	11.7043	1.666	11.0727	1.852	12.3036
^{168}Hf	96	0.254	3.110	2.723	1.925	11.4514	1.808	10.7525	2.036	12.1100
^{170}Hf	98	0.274	3.194	2.951	2.087	11.5505	1.950	10.7923	2.215	12.2620
^{172}Hf	100	0.284	3.248	3.211	2.271	12.1492	2.116	11.3223	2.415	12.9233
^{174}Hf	102	0.285	3.268	3.381	2.391	12.7500	2.227	11.8765	2.544	13.5673
^{176}Hf	104	0.277	3.284	3.572	2.526	13.8379	2.356	12.9067	2.685	14.7102
^{178}Hf	106	0.278	3.291	3.668	2.594	14.1614	2.418	13.2047	2.758	15.0575
^{180}Hf	108	0.279	3.307	4.039	2.856	15.5409	2.662	14.4843	3.038	16.5301
^{182}Hf	110	0.270	3.295	3.741	2.645	14.8479	2.470	13.8656	2.809	15.7691
^{184}Hf	112	0.260	3.264	3.341	2.362	13.7428	2.212	12.8652	2.504	14.5677

Table 12
The same as in Table 1 but for the isotopic chain of Os($Z = 76$). For ^{162}Os the nuclear deformation β is too small to provide acceptable results such that one considered and listed for this nucleus the nuclear deformation corresponding to the linear fit from Fig. 7 performed for the rest of the data points.

Nucleus	N	β	$R_{4/2}$	ρ	d	k	d_p	k_p	d_n	k_n
^{162}Os	86	0.104	1.990	1.273	0.900	12.6183	0.989	13.8670	0.801	11.2315
^{164}Os	88	0.107	2.201	1.702	1.203	16.4108	1.207	16.4600	1.200	16.3615
^{166}Os	90	0.134	2.363	1.887	1.334	14.6318	1.310	14.3631	1.358	14.8956
^{168}Os	92	0.162	2.513	2.032	1.437	13.1245	1.391	12.7101	1.481	13.5263
^{170}Os	94	0.171	2.616	2.127	1.504	13.0435	1.449	12.5678	1.557	13.5025
^{172}Os	96	0.190	2.661	2.170	1.534	12.0303	1.470	11.5276	1.596	12.5129
^{174}Os	98	0.226	2.743	2.247	1.589	10.5579	1.508	10.0196	1.666	11.0700
^{176}Os	100	0.246	2.927	2.444	1.728	10.5948	1.629	9.9851	1.822	11.1713
^{178}Os	102	0.247	3.017	2.562	1.812	11.0637	1.705	10.4139	1.912	11.6773
^{180}Os	104	0.238	3.093	2.689	1.901	12.0285	1.792	11.3341	2.005	12.6849
^{182}Os	106	0.239	3.155	2.828	2.000	12.6000	1.883	11.8623	2.110	13.2969
^{184}Os	108	0.229	3.203	2.985	2.111	13.8507	1.990	13.0604	2.225	14.5982
^{186}Os	110	0.220	3.165	2.856	2.019	13.7673	1.909	13.0129	2.124	14.4825
^{188}Os	112	0.192	3.083	2.671	1.889	14.6604	1.798	13.9570	1.975	15.3316
^{190}Os	114	0.164	2.934	2.452	1.734	15.6518	1.664	15.0254	1.801	16.2540
^{192}Os	116	0.155	2.376	1.900	1.344	12.8041	1.311	12.4937	1.375	13.1072
^{194}Os	118	0.145	2.750	2.255	1.595	16.2040	1.542	15.6701	1.645	16.7209
^{196}Os	120	−0.156	2.533	−2.051	−1.450	12.4469	−1.551	13.3137	−1.342	11.5151
^{198}Os	122	−0.096	2.307	−1.828	−1.293	18.4353	−1.367	19.4936	−1.214	17.3124

Recalling that ρ is determined by fitting the ratio $R_{4/2}$ and replacing the l.h.s. of the above equation with the corresponding experimental value one obtains a second degree algebraic equation for the ratio d_p/k_p. Considering Eq. (3.21) for protons with the value of d_p/k_p just determined, one gets an equation for β. From here determining d_n and k_n is an obvious procedure. Results obtained with this method for the already mentioned set of 5 nuclei are collected in Table 16.

Another issue addressed in this paper regards the ability of the model proposed to describe the shell filling and how that compares with what we know from the Nilsson model. To this aim we calculated the second order binding energy difference

$$\Delta E_{Tot} = -\frac{3}{16}\left[2E(N) - E(N+2) - E(N-2)\right], \tag{5.5}$$

Table 13
The same as in Table 1 but for the isotopic chain of Pt($Z = 78$). For ^{200}Pt and ^{202}Pt the nuclear deformation β is too small to provide acceptable results such that for these nuclei one considered and listed the nuclear deformation corresponding to the linear fit from Fig. 7 performed for the rest of the data points.

Nucleus	N	β	$R_{4/2}$	ρ	d	k	d_p	k_p	d_n	k_n
^{168}Pt	90	−0.096	2.249	−1.761	−1.245	17.7596	−1.324	18.8764	−1.162	16.5677
^{170}Pt	92	0.107	2.301	1.822	1.288	17.5679	1.279	17.4395	1.298	17.6953
^{172}Pt	94	0.126	2.338	1.861	1.316	15.3147	1.296	15.0878	1.335	15.5383
^{174}Pt	96	0.153	2.262	1.777	1.257	12.1257	1.237	11.9356	1.276	12.3129
^{176}Pt	98	0.171	2.137	1.611	1.139	9.8792	1.137	9.8563	1.142	9.9020
^{178}Pt	100	0.254	2.510	2.029	1.435	8.5328	1.361	8.0953	1.505	8.9489
^{180}Pt	102	0.265	2.681	2.188	1.547	8.8392	1.458	8.3303	1.631	9.3203
^{182}Pt	104	0.255	2.708	2.213	1.565	9.2720	1.477	8.7514	1.648	9.7649
^{184}Pt	106	0.247	2.675	2.182	1.543	9.4227	1.460	8.9140	1.622	9.9053
^{186}Pt	108	0.239	2.560	2.076	1.468	9.2495	1.395	8.7890	1.538	9.6881
^{188}Pt	110	−0.164	2.526	−2.044	−1.445	11.7627	−1.551	12.6240	−1.331	10.8331
^{190}Pt	112	−0.156	2.492	−2.012	−1.423	12.2103	−1.524	13.0785	−1.314	11.2753
^{192}Pt	114	−0.156	2.479	−2.000	−1.414	12.1374	−1.515	13.0065	−1.305	11.2011
^{194}Pt	116	−0.148	2.470	−1.992	−1.409	12.7817	−1.505	13.6591	−1.305	11.8394
^{196}Pt	118	−0.139	2.465	−1.987	−1.405	13.6218	−1.497	14.5099	−1.307	12.6716
^{198}Pt	120	−0.139	2.419	−1.943	−1.374	13.3202	−1.466	14.2161	−1.279	12.3595
^{200}Pt	122	−0.180	2.347	−1.870	−1.322	9.7430	−1.440	10.6067	−1.194	8.7949
^{202}Pt	124	−0.180	2.344	−1.867	−1.320	9.7274	−1.437	10.5916	−1.191	8.7785

Table 14
The same as in Table 1 but for the isotopic chain of Th($Z = 90$). For few nuclei, ^{214,218,220}Th, the nuclear deformation β is too small to provide acceptable results. For these nuclei one considered the nuclear deformation, β^{fit}, corresponding to the linear fit from Fig. 7 performed for the rest of the data points. The experimental ratio $R_{4/2}$ for ^{218}Th is not much smaller than the minimum theoretical value 1.954 hence one adopted for it the corresponding minimum value $\rho = 0.930$. The horizontal line indicates the change of neutron shell model parameters κ and μ.

Nucleus	N	β	β^{fit}	$R_{4/2}$	ρ	d	k	d_p	k_p	d_n	k_n
^{214}Th	124	−0.052	−0.111	2.332	−1.855	−1.312	16.0918	−1.392	17.0779	−1.226	15.0411
^{216}Th	126	0.008		1.227							
^{218}Th	128	0.008	0.056	1.732	0.930	0.658	16.8913	0.884	22.6978	0.290	7.4458
^{220}Th	130	0.030	0.085	2.035	1.416	1.001	17.0840	1.060	18.0800	0.939	16.0263
^{222}Th	132	0.111		2.399	1.923	1.360	17.8927	1.340	17.6360	1.379	18.1457
^{224}Th	134	0.164		2.896	2.407	1.702	15.3645	1.635	14.7567	1.767	15.9492
^{226}Th	136	0.173		3.136	2.782	1.967	16.8710	1.880	16.1244	2.051	17.5860
^{228}Th	138	0.182		3.235	3.130	2.213	18.0814	2.108	17.2250	2.313	18.8990
^{230}Th	140	0.198		3.271	3.408	2.410	18.1638	2.286	17.2308	2.528	19.0512
^{232}Th	142	0.207		3.284	3.563	2.519	18.2014	2.385	17.2280	2.647	19.1253
^{234}Th	144	0.215		3.291	3.669	2.594	18.0777	2.451	17.0786	2.730	19.0245

Table 15
The same as in Table 1 but for the isotopic chain of U($Z = 92$). For ^{240}U the experimental ratio $R_{4/2}$ exceeds its asymptotic value 3.33, such that for this nucleus one considered and listed the value of ρ interpolated by the linear fit from Fig. 7 for the corresponding β.

Nucleus	N	β	$R_{4/2}$	ρ	d	k	d_p	k_p	d_n	k_n
^{230}U	138	0.199	3.274	3.436	2.430	18.2252	2.304	17.2844	2.549	19.1197
^{232}U	140	0.207	3.291	3.670	2.595	18.7480	2.456	17.7435	2.727	19.7014
^{234}U	142	0.215	3.296	3.762	2.660	18.5360	2.513	17.5101	2.800	19.5080
^{236}U	144	0.215	3.304	3.958	2.799	19.5017	2.643	18.4198	2.946	20.5266
^{238}U	146	0.215	2.303	3.950	2.793	19.4623	2.638	18.3827	2.940	20.4850
^{240}U	148	0.229	3.347	4.004	2.831	18.5790	2.666	17.4942	2.987	19.6038

with $E(N)$ denoting the total sum of proton and neutron single particle energies for a nucleus with N neutrons. This quantity is plotted for the isotopic chains of Cd and Te in Fig. 8. We notice that

Table 16
Results for deformation parameters and canonicity constants obtained with a different algorithm than that used in the previous tables: The ratio d_p/k_p is fixed such that the experimental value of the quadrupole moment of the state 2^+, Q_2^{Exp}, is reproduced by Eq. (5.4). ρ is determined by fitting the ratio $R_{4/2}$ and then Eq. (3.21) provides β_2. The remaining parameters are fixed following the same path as for the other nuclei.

Nucleus	$Q_0^{Exp}[eb]$	$R_{4/2}$	β_2	ρ	d	k	d_p	k_p	d_n	k_n
^{72}Ge	−0.13(6)	2.072	0.237	1.498	1.059	6.7358	1.061	6.7460	1.058	6.7257
^{116}Cd	−0.42(4)	2.375	0.368	1.899	1.343	5.6322	1.255	5.2655	1.425	5.9765
^{122}Te	−0.57(5)	2.094	0.441	1.540	1.089	3.8476	1.046	3.6950	1.131	3.9945
^{124}Te	−0.45(5)	2.072	0.348	1.497	1.059	4.6786	1.038	4.5896	1.078	4.7659
^{126}Te	−0.20(9)	2.043	0.155	1.435	1.015	9.6735	1.050	10.005	0.979	9.3297

Table 17
With the nuclear deformation β taken for Ref. [46] and the deformation parameters as well as the canonicity constants determined as discussed in the text we determined the quantum numbers $[Nlj1]$ of the last occupied (Locc), the second last occupied (Slocc) and the first unoccupied (Funocc) neutron states of several even–odd isotopes. Presuming that the Fermi sea is close to one of the mentioned states we can get information upon the spin of the ground state of the odd system whose experimental values (see [15] p. 78) are listed on the last column. Indeed in the region of the last occupied state the level density is high which results that the odd nucleon position is sensitive to the residual interaction.

Nucleus	β_2	ρ	d	k	d_p	k_p	d_n	k_n	Locc	Slocc	Funocc	I_{Exp}
^{155}Gd	0.252	2.939	2.078	12.4534	1.951	11.6878	2.199	13.1745	$[66\frac{13}{2}\frac{1}{2}]$	$[55\frac{9}{2}\frac{3}{2}]$	$[66\frac{13}{2}\frac{3}{2}]$	$\frac{3}{2}$
^{157}Gd	0.271	3.161	2.235	12.5011	2.088	11.6810	2.373	13.2707	$[66\frac{13}{2}\frac{1}{2}]$	$[55\frac{9}{2}\frac{3}{2}]$	$[66\frac{13}{2}\frac{5}{2}]$	$\frac{3}{2}$
^{167}Er	0.294	3.697	2.614	13.5377	2.430	12.5842	2.786	14.4282	$[53\frac{7}{2}\frac{5}{2}]$	$[55\frac{9}{2}\frac{5}{2}]$	$[66\frac{13}{2}\frac{7}{2}]$	$\frac{7}{2}$
^{177}Hf	0.277	3.403	2.406	13.1820	2.245	12.2975	2.557	14.0107	$[53\frac{5}{2}\frac{1}{2}]$	$[51\frac{3}{2}\frac{1}{2}]$	$[55\frac{9}{2}\frac{7}{2}]$	$\frac{7}{2}$
^{179}Hf	0.278	3.415	2.415	13.1845	2.252	12.2973	2.567	14.0157	$[55\frac{9}{2}\frac{7}{2}]$	$[53\frac{5}{2}\frac{1}{2}]$	$[66\frac{13}{2}\frac{9}{2}]$	$\frac{9}{2}$
^{187}Os	0.212	2.588	1.830	12.9232	1.735	12.2539	1.920	13.5595	$[53\frac{7}{2}\frac{7}{2}]$	$[53\frac{5}{2}\frac{1}{2}]$	$[55\frac{9}{2}\frac{9}{2}]$	$\frac{1}{2}$
^{189}Os	0.183	2.234	1.580	12.8377	1.514	12.3051	1.643	13.3491	$[55\frac{9}{2}\frac{9}{2}]$	$[53\frac{5}{2}\frac{1}{2}]$	$[66\frac{13}{2}\frac{11}{2}]$	$\frac{1}{2}$

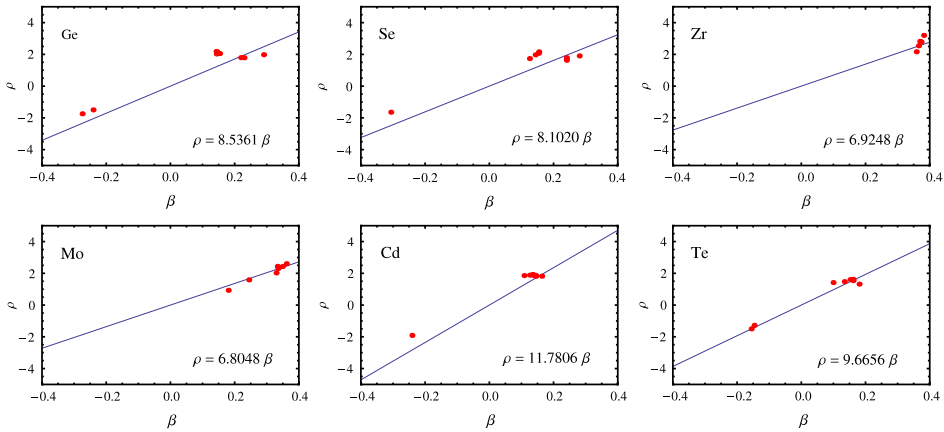

Fig. 6. Linear fits with vanishing intercept of the tabulated nuclear deformation β as a function of the global deformation parameter ρ obtained by reproducing the experimental value of the $R_{4/2}$ ratio, by means of Eq. (4.6), are presented for the lightest isotopic chains. The data points with $\beta = 0$ or very small are excluded from the fit.

both models show two major peaks corresponding to the magic number 82 and the shell filling at $N = 68$ for Cd and $N = 70$ for Te. The distributions of peaks for Te isotones obtained with the projected spherical single particle basis (PSSPB) and the Nilsson model respectively, are similar. Some differences appear in the case of Cd's. In the case of Nilsson plot there is a peak for $N = 76$ which is missing in our case. On the other hand the plot with PSSPB exhibits a peak for $N = 56$ which is

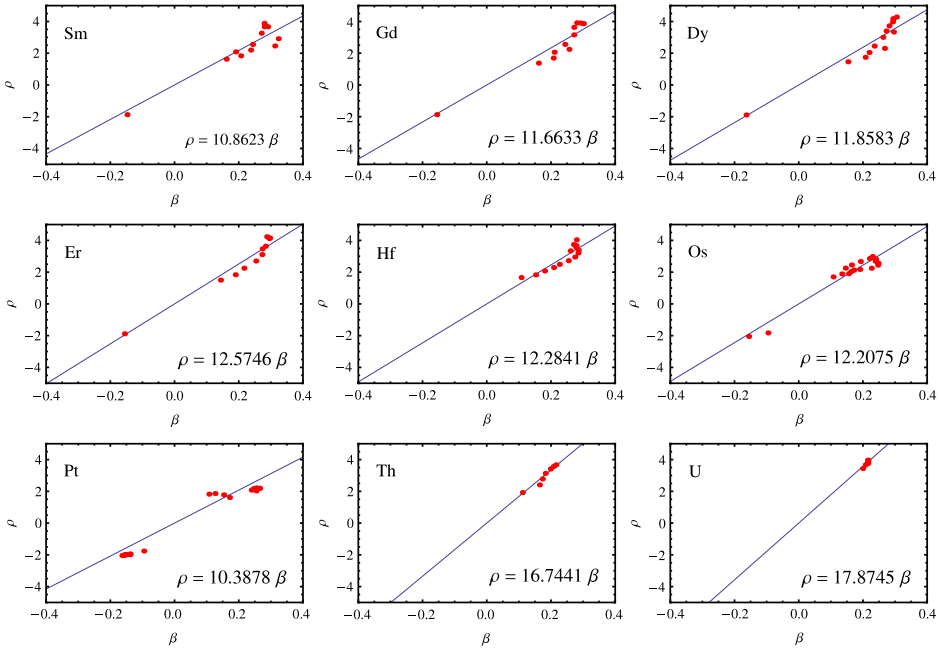

Fig. 7. Linear fits with vanishing intercept of the tabulated nuclear deformation β as a function of the global deformation parameter ρ obtained by reproducing the experimental value of the $R_{4/2}$ ratio, by means of Eq. (4.6), are presented for the heavier isotopic chains. The data points with $\beta = 0$ or very small and with $R_{4/2} > 3.33$ (^{240}U) are excluded from the fit.

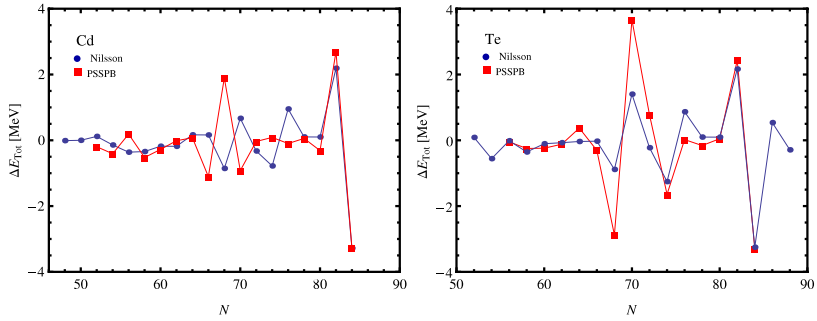

Fig. 8. The binding energy second order difference, ΔE_{Tot} for the isotopes of Cd (left panel) and Te (right panel) is represented as a function of the number of neutrons, N. For Nilsson model calculations we included also the $\Delta N = 2$ matrix elements with $N_{cutoff} = 10$.

missing in the case of the plot made with the Nilsson model. The major peak at $N = 70$ for the Nilsson model is shifted to $N = 68$ for our method.

The order of the shell filling is, of course, depending on the quadrupole deformation. A test for this feature is to identify the levels around the last occupied one and compare their spin with the experimental value for the ground state spin, in an even–odd nucleus. The results are compared with the data for a few odd nuclei in Table 17. Among the identified angular momenta for the last and the second last occupied as well as for the first unoccupied levels one finds the angular momenta characterizing the ground state according to the experimental data. The reason we listed all three spins is that in the region of the Fermi sea the level density is high and a small uncertainty in determining the deformation may change the position of the level crossing and thus the filling order. Moreover

our estimation does not take into consideration the effect of the residual interaction which may also shift the position of the Fermi level. We note that the agreement is reasonably good suggesting that the ground state has the spin of the first unoccupied level for ^{155}Gd, ^{167}Er, ^{177}Hf, ^{179}Hf and that of the second last occupied state for ^{187}Os, ^{189}Os, ^{157}Gd.

The results concerning the canonicity parameters k, k_p and k_n for the 194 isotopes can be interpolated by linear functions of the atomic mass number A.

$$k = 0.0513471 \cdot A + 4.28957, \quad rms = 2.59477, \tag{5.6}$$

$$k_p = 0.0488292 \cdot A + 4.61187, \quad rms = 2.71376, \tag{5.7}$$

$$k_n = 0.0538922 \cdot A + 3.80843, \quad rms = 3.17185. \tag{5.8}$$

Given the large number of the isotopes considered, the interpolation accuracy is reasonably good. This can however be improved if an additional dependence on Z is introduced. The above equations can be used for the isotopes not included in Tables 1–15 to determine the deformation parameters d, d_p and d_n following a shortcut of the algorithm described above.

Knowing the deformation d for a chosen nucleus, one can investigate its shape by calculating the total nucleon density as a function of the stretched radial coordinate r' and the azimuthal angle θ. Note that due to the assumed axial symmetry of the nucleus, the nucleon density is independent of the polar angle φ. For illustration, one considers two isotopes of Gd which are sizeable distinguished by the values of both the nuclear deformation β and the isospin independent deformation parameter d. The chosen isotopes are ^{150}Gd with $\beta = 0.161$ and $d = 0.971$, and ^{156}Gd with $\beta = 0.271$ and $d = 2.232$, the deformation parameters being those from Table 8.

Keeping in mind our declared aim of comparing the spherical projected single-particle basis with the projected Nilsson states, the total nuclear density in the spherical shell model is the common feature of the two projected spherical bases. This quantity is plotted in Fig. 9 for the two nuclei ^{150}Gd and ^{156}Gd. In order to fully represent an axial section of the nuclei, the domain for θ was extended from $[0, \pi]$ to $[0, 2\pi]$.

Since the density in the spherical shell model does not depend on deformation, being rotationally symmetric, the graphs shown in Fig. 9 for the two nuclei are almost identical. The only difference is caused by the additional occupied single-particle states, whose contribution stays in the outer layers of the nucleus ^{156}Gd, around $r' = 1.5 - 2.5$.

In Fig. 10 one depicted the projected total nuclear density given by Eq. (3.25) normalized to its maximum value for the two considered Gd isotopes as functions of the same variables as in Fig. 9. Such a normalization is necessary in order to have the same scale for both nuclei given the fact that the absolute values for the two nuclei are different due to the nonorthogonality of the involved projected state (3.26). Now the difference between the two nuclei is conspicuous. Indeed, for the less deformed nucleus ^{150}Gd, the density probability (3.25) is mostly distributed in the center with a small extension radius, while in the case of the more deformed nucleus ^{156}Gd, the same density covers a broader space which does not have a spherical symmetry, approximately satisfied in the first case. The specific manner of inducing the deformation effect seems to determine a slight hexadecapole deformation due to squaring the expression (3.26) which already includes the quadrupole deformation.

In Fig. 11 the nucleon density corresponding to the Nilsson model and determined by Eq. (3.28), is plotted as a function of $r' \cos\theta$ and $r' \sin\theta$. Comparing it with the density averaged with the quadrupole coherent state, given by Eq. (3.25), one may detect the nuclear deformation effect. Indeed, the two sets of pictures resemble with each other in many respects the differences regarding the inner part corresponding to a high density which in the case of Fig. 11 is more deformed along the axis $r' \cos\theta$. Thus, we may say that the deformation affects mainly the nuclear core, the outer shells keeping the spherical symmetry. If you look carefully to the section of the nucleon density presented in Fig. 11 one notices a slight distortion of equidensity levels, in the high density region, along the axis $r' \sin\theta$. The slight hexadecapole distortion might be caused by the inclusion of the $\Delta l = 2$ matrix elements in the diagonalization procedure used for determining the eigenstates. A similar effect, but in a more pronounced manner, is seen in the density plotted in Fig. 10 by means of Eq. (3.25).

Studying some contour lines made at very high values of the nucleon density for both nuclei, in Fig. 12 it is found that the elongated oval shape is preserved when the density is increased, in the case

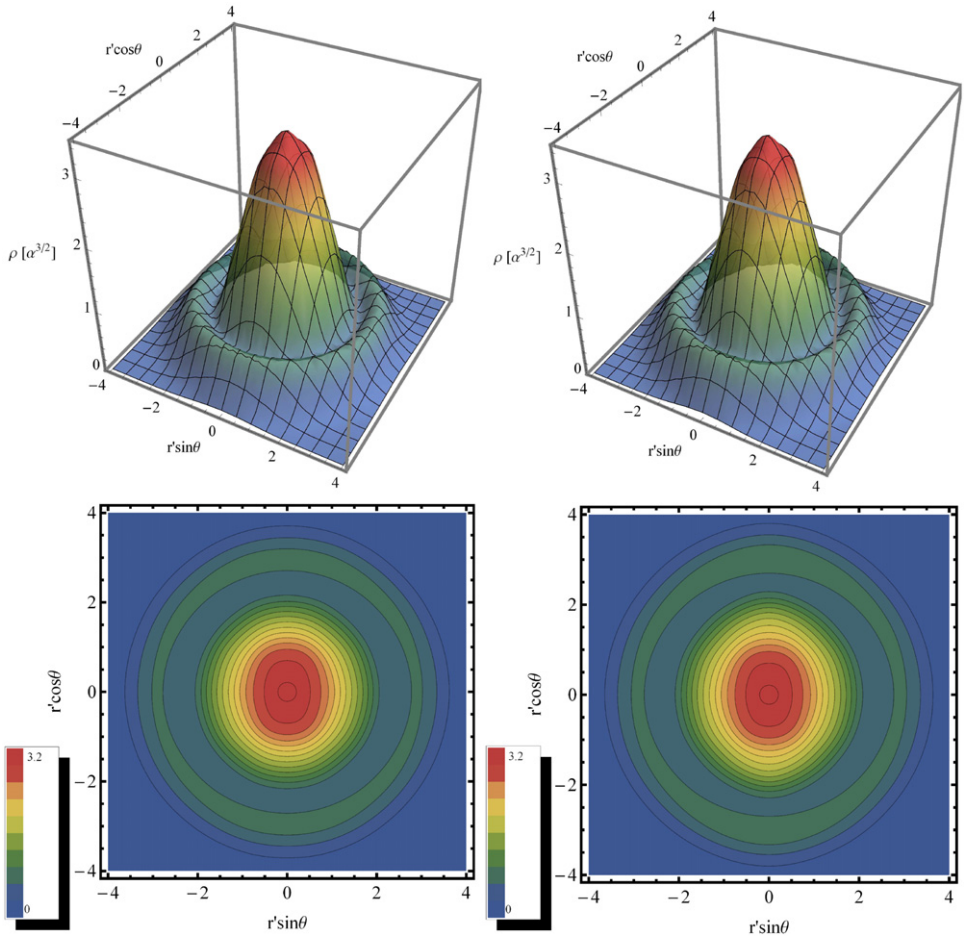

Fig. 9. Total nuclear density given by Eq. (3.24) is represented as a function of $x = r' \sin\theta$ and $z = r' \cos\theta$ in units of $\alpha^{\frac{3}{2}}$ in 3D plots (up) and contour plots (down) for ^{150}Gd (left) and ^{156}Gd (right). In both cases the densities corresponding to two adjacent curves differ from each other by $0.21\alpha^{3/2}$.

of the less deformed nucleus ^{150}Gd, while for ^{156}Gd the presence of the two peaks shown in the upper right part of Fig. 11 is reflected in Fig. 12 by a neck which is more pronounced for higher density. The full separation of the two peaks for very high density is translated in the contour line plot by two disconnected drops.

Concluding, here we studied the nucleon density described by the projected spherical single particle basis and compared the results with those corresponding to the Nilsson model. Also, the effect of deformation on the nucleon density was pointed out by comparing the results for a near spherical isotope, ^{150}Gd, and a well deformed one ^{156}Gd.

Before closing this section it is worth mentioning two approaches to treat a many body system with a projected spherical basis. One is called the projected shell model (PSM) [55] and treats a many body Hamiltonian consisting in a Nilsson mean field term, the pairing and the QQ interactions. The first two terms define, through the BCS approach, the space of 0, 2, 4, . . . , quasiparticles. For a given angular momentum, the Hamiltonian was diagonalized in the basis of projected states corresponding to the deformed quasiparticle states. The application was made not only for medium nuclei like ^{48}Cr but also for some heavy isotopes, ^{178}Hf, ^{254}No. A similar approach, but for a different deformed mean field was employed in Refs. [56,57] to study the single and multi-backbending phenomena. Note that while

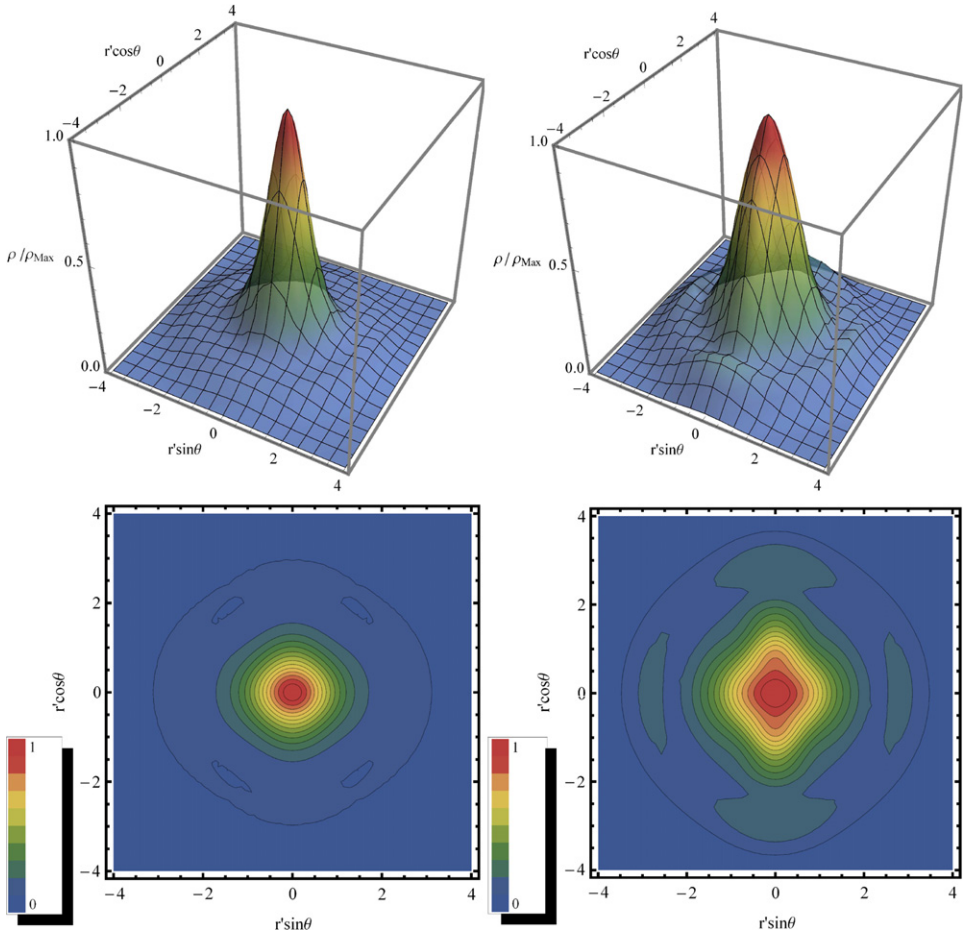

Fig. 10. Total nuclear density projected on the quadrupole boson coherent state defined by Eq. (3.24) and normalized to its maximum value is represented as a function of $x = r' \sin\theta$ and $z = r' \cos\theta$ in 3D plots (up) and contour plots (down) for ^{150}Gd (left) and ^{156}Gd (right). Contour plots are made with a step of $0.062/\rho_{max}$.

in the quoted papers a projected spherical basis is obtained from a deformed many body basis, we propose a projected single particle basis to treat, in a unified fashion, the spherical and the deformed many body systems. According to the arguments presented here our procedure seems to be simpler than the PSM. Moreover, the system angular momentum described by PSM is limited and depends on the input data for the number of particles involved. By contrast, here the core angular momentum is unlimited being carried by bosons. Alternatively, starting with a many body Hamiltonian [58], one defines a body fixed reference frame which allows to separate two subsystems, a collective core described by an axially symmetric rotor and a set of intrinsic single particle states. The approximated Hamiltonian was treated in a product particle–core basis where the angular momentum is carried exclusively by the core's factor function. The ansatz for the particle factor function is an axially symmetric Hartree–Fock state plus a two quasiparticle excitation of it. System energies are obtained by averaging the particle–rotor Hamiltonian with an arbitrary component of the product basis. It is interesting to note that inserting the asymptotic expression for the core projected function $\phi_J^{(c)}$, as given in Ref. [19], the particle–core basis (3.13) resembles the particle–rotor basis used in [58]. Moreover, when the space of intrinsic functions is restricted to one state, the particle–rotor method can be used to define a mean field for the particle motion and moreover a projected spherical basis.

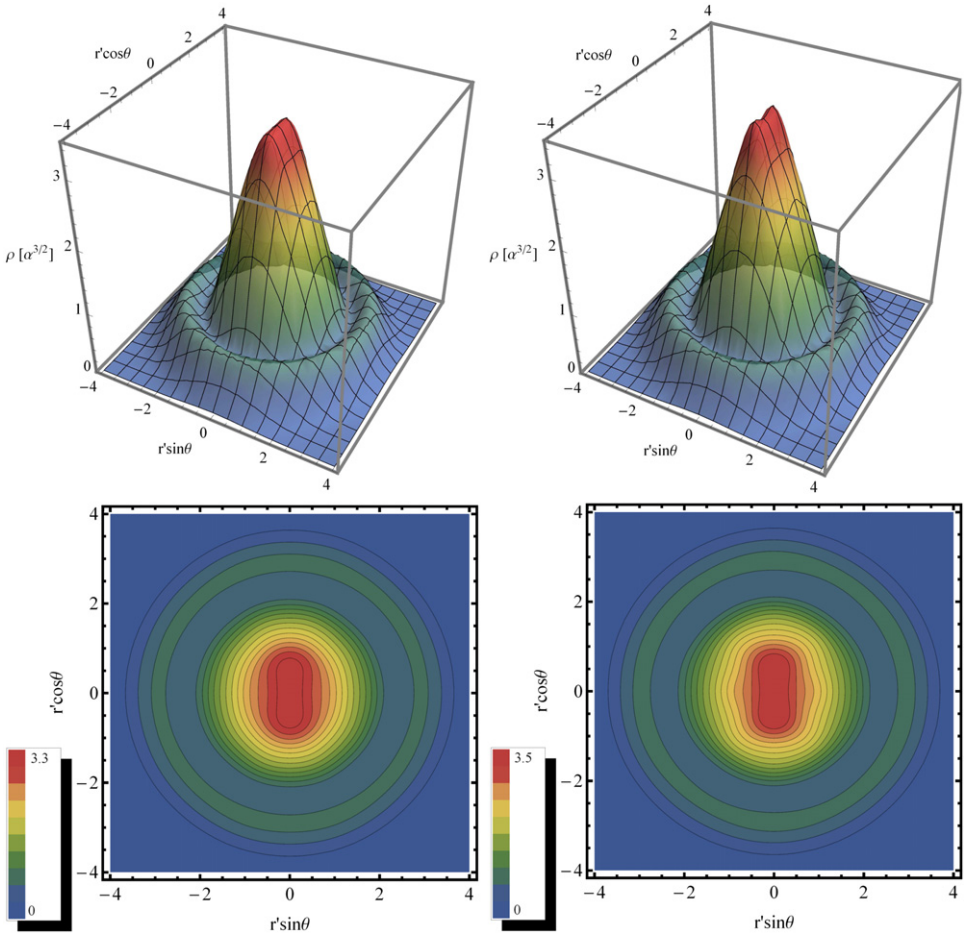

Fig. 11. Total nuclear density in the Nilsson model given by Eq. (3.28) is represented as a function of $x = r' \sin\theta$ and $z = r' \cos\theta$ in units of $\alpha^{\frac{3}{2}}$ in 3D plots (up) and contour plots (down) for ^{150}Gd (left) and ^{156}Gd (right). Contour plots are made with a step of $0.21\alpha^{3/2}$.

Actually these are only two examples of many others, which attempt to define the optimal basis for treating complex systems like many body or particle–core systems. The examples prove the importance of the treated subject as well as the simplicity of the proposed solution.

6. Conclusions

Results of the present work can be summarized as follows. Besides the nuclear shell model parameters, the projected single particle basis involves another two, namely the deformation parameter d and the constant k entering the canonical transformation relating the quadrupole coordinates with the boson operator. When some tuning properties which are isospin dependent are concerned, the single particle projected basis for protons and neutrons should be different and consequently different parameters d and k are to be used. The isospin dependence of these parameters is underlined by using different notations for them, when they are involved in the equation for protons, d_p and k_p, and neutrons, d_n and k_n, respectively. The algorithm of fixing these parameters is defined by several steps: (a) By equating the theoretical result for the ratio $R_{4/2}$ to the experimental value, one obtains a rela-

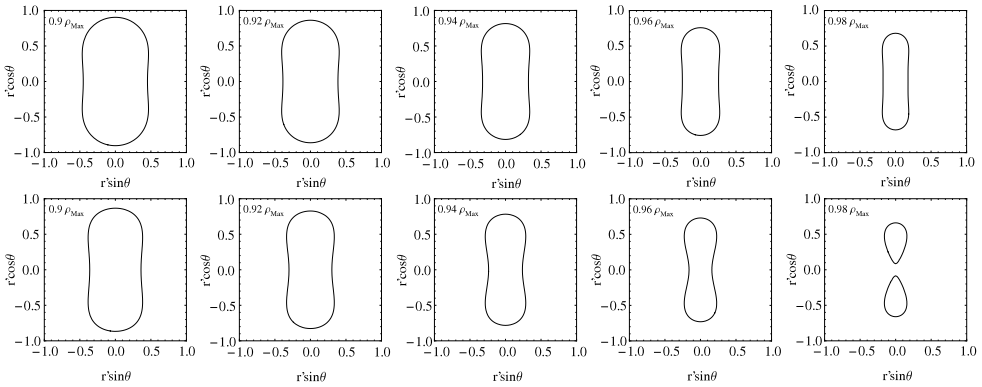

Fig. 12. Contour lines of constant and very high density in the Nilsson model, given by Eq. (3.28), is represented as a function of $x = r' \sin\theta$ and $z = r' \cos\theta$ in units of $\alpha^{\frac{3}{2}}$ for ^{150}Gd (up) and ^{156}Gd (down).

tion determining the global deformation $\rho(= d\sqrt{2})$ (4.3); (b) Inserting d in Eq. (3.21) the parameter k is readily obtained; (c) From the expression of the $B(E2)$ value associated to the transition $0^+ \to 2^+$ the parameter k_p is obtained; (d) Using again Eq. (3.21) corresponding to the proton system, the deformation parameter d_p is calculated; (e) From Eq. (4.3) we determine d_n; (f) Eq. (3.21) for neutrons finally determines k_n.

This procedure was applied to 194 isotopes and the resulting parameters are listed in Tables 1–15. For 186 isotopes, the quadrupole deformation involved in Eq. (3.21) is taken from Ref. [46]. For the remaining eight isotopes the quadrupole deformation from Ref. [46] provides a wrong sign for the quadrupole moment of the lowest state 2^+. In order to correct for this drawback we slightly changed the procedure of fixing the involved parameters. Indeed, for three isotopes, ^{74}Ge, ^{74}Se and ^{76}Se, we inserted for β the corresponding experimental values from Refs. [51–53], otherwise kept the same algorithm as before. As for the last five nuclides, ^{72}Ge, ^{116}Cd, ^{122,124,126}Te, the fitting procedure is as follows: (a) Inserting ρ, fixed by fitting the ratio $R_{4/2}$, in the defining equation of Q_2 (5.4), this becomes an equation for d_p/k_p; (b) Considering Eq. (3.21) for protons with the ratio d_p/k_p just determined, one obtains an equation for β; (c) Knowing ρ, one calculates d and from (3.21), k; (d) With d and d_p, the deformation d_n is readily obtained; (e) Again, Eq. (3.21) for neurons determines k_n. In this way the signs of 50 experimental values for Q_2 [54] are reproduced.

The specific behavior of the neutron system when either a magic number or a single shell filling are approached is studied by plotting the second order difference of the system binding energy as a function of the neutron number for Cd and Te isotopes. Identifying the quantum numbers for the last and second last occupied as well as the first unoccupied states for an even–odd nucleus, one may say what the ground state spin could be. The comparison with experimental data may indicate the correctness of the shell filling order. For the selected nuclei in Table 17 the agreement obtained is quite good.

The ratio $R_{4/2}$ represented as a function of ρ exhibits a flat minimum in the beginning of the considered interval then a transitional region and finally a plateau is reached in the asymptotic region of the deformation. For isotopes where the experimental mentioned ratio is below the calculated minimum as well as for those characterized by experimental values larger than the rotational limit of 3.33, this algorithm cannot be applied. The domain of ρ where the ratio is unambiguously defined and employed in solving the equation determining ρ is [0.930, 5].

The results of ρ for fifteen isotopic chains are plotted as a function of the nuclear deformation β and then the bulk of points interpolated by a straight line. There are few isotopes where the nuclear deformation is very close to zero and consequently Eq. (3.21) cannot be used. In these cases the linear interpolation is used to determine a new deformation parameter called β^{fit} considered to be the deformation which corresponds to the known ρ.

One aim of this paper consists of making explicit the relationship between the projected spherical single particle basis and the basis of the Nilsson model. The comparison is made in terms of the predicted single particle energies and nucleon density. The detailed comparison supply us with the results: (i) If one diagonalizes the Nilsson Hamiltonian in a spherical shell model basis with $\Delta N = 0$ then projecting out the good angular momentum, the spherical shell model state is obtained. Averaging now the Hamiltonian with the resulting projected spherical Nilsson' s state one obtains an analytical expression for energies denoted by $\epsilon^{Nilss}_{nlj\Omega}$ (2.9). These energies are compared with those characterizing the projected spherical single particle basis (3.22) in Figs. 3 and 4. As may be seen the two sets of energies are almost identical; (ii) The projected spherical single particle basis (3.13) and the projected Nilsson basis yield identical nucleon density with that associated to the spherical shell model (see Fig. 9). This was actually expected due to the common rotational symmetries; (iii) However, the deformation can be implemented by averaging the result on the coherent state of the core (3.25). This is represented as both a 3D and a contour plot for two isotopes of Gd, ^{150}Gd and ^{156}Gd, in Fig. 10. Since the density is obtained by squaring the modulus of the wave function which includes already a quadrupole deformation a high order like hexadecapole deformation effect is seen. Similar plots are performed in Fig. 11 for the density provided by the Nilsson states (3.28). The effect of hexadecapole deformation is seen in the 3D plot by the split of the peak seen for high density as well as in the contour plot where some equidensity curves are stretched along both the $r'cos\theta$ and the $r'sin\theta$ axes. For inner shells the stretching along the $r'sin\theta$ axis is changed to a compressing effect. This is shown in Fig. 12 where the contour lines are plotted for very high density. For the more deformed isotope, i.e. ^{156}Gd, the effect is more evident, the contour shape resembling that of a lens grain. Increasing the density, the neck is shrunk ending by the extreme shape of two disconnected drops. An equation relating the k-pole transition densities defined by the spherical shell model and the projected spherical basis respectively, is analytically derived (3.33).

In several places it is commented why the particle–core projected basis can be used as a single particle basis. Indeed, it was underlined the fact that the role of the core factor function is to generate the deformation. Thus, the matrix elements of a particle-like operator between two states of the new basis are factorized, one factor carrying the deformation while the other one being just the matrix element between the corresponding spherical shell model states. It is amazing that the projected spherical basis can be used also for many body calculations, although each particle has its own core. In Ref. [40] we have proved that the matrix elements of a two body interaction between two pairs of projected states are very close to the matrix elements of the same interaction between two states, each of them consisting of two single particle shell model states and a common core wave function. Due to this property the present procedure might be compared with some powerful many body formalisms like the PSM [55] and the particle–rotor model [58]. As a matter of fact this basis was used to microscopically describe the scissor like and spin-flip states [40] as well as for calculating the transition rate of a double beta decay [59–62].

Concluding, the results of this paper prove that the projected spherical single particle basis is an efficient tool for describing, in a unified fashion, the spherical and deformed nuclei.

Acknowledgment

This work was supported by the Romanian Ministry for Education Research Youth and Sport through the CNCSIS project ID-2/5.10.2011.

References

[1] M. Baranger, K. Kumar, Nucl. Phys. A 110 (1968) 490; Nucl. Phys. A 122 (1968) 273.
[2] D. Janssen, R.V. Jolos, F. Donau, Nucl. Phys. A 224 (1974) 93.
[3] S.G. Nilsson, Dan. Mat. Fys. Medd. 16 (1955) 29.
[4] A.A. Raduta, V. Ceausescu, G. Stratan, A. Sandulescu, Phys. Rev. C 8 (1973) 1525.
[5] V. Ceausescu, A.A. Raduta, Progr. Theoret. Phys. 52 (1974) 903.
[6] S.E. Koonin, D.J. Dean, K. Langanke, Phys. Rep. 278 (1997) 1.
[7] G. Holzwarth, Nucl. Phys. A 156 (1970) 511; Nucl. Phys. A 174 (1971) 97.
[8] T. Kishimoto, T. Tamura, Nucl. Phys. A 270 (1976) 317.
[9] A. Bohr, B. Mottelson, Dan. Mat. Fys. Medd. 26 (1952) 1.
[10] A. Faessler, W. Greiner, Z. Phys. 168 (1962) 425.

[11] A. Faessler, W. Greiner, Z. Phys. 170 (1962) 105.
[12] A. Faessler, W. Greiner, Z. Phys. 177 (1964) 190.
[13] P. Hess, J. Maruhn, W. Greiner, J. Phys. G 7 (1981) 737.
[14] J.M. Eisenberg, W. Greiner, Nuclear Theory, Vol. 3, second ed., North-Holland, Amsterdam, 1976.
[15] P. Ring, P. Schuck, The Nuclear Many-body Problem, Springer-Verlag, 1980.
[16] A.S. Davydov, G.F. Filippov, Nuclear Phys. 8 (1958) 788.
[17] L. Wilets, M. Jean, Phys. Rev. 102 (1956) 788.
[18] S.A. Moszkowski, Phys. Rev. 110 (1958) 403.
[19] A.A. Raduta, V. Ceausescu, A. Gheorghe, R.M. Dreizler, Nucl. Phys. A 381 (1982) 253.
[20] A.A. Raduta, R.M. Dreizler, Nucl. Phys. A 258 (1976) 109.
[21] A.A. Raduta, V. Ceausescu, A. Faessler, Rev. Roum. Phys. 31 (1986) 649.
[22] A.A. Raduta, A. Faessler, V. Ceausescu, Phys. Rev. C 36 (1987) 2111.
[23] R.E. Peierls, J. Yokoz, Proc. Phys. Soc. (London) A 70 (1957) 381.
[24] N. Onishi, S. Yoshida, Nucl. Phys. 80 (1966) 367.
[25] H.J. Mang, Phys. Rep. 18 (1975) 325.
[26] N. Onishi, J.W. Negele, Nucl. Phys. A 301 (1978) 336.
[27] K.W. Schmid, F. Grümmer, A. Faessler, Phys. Rev. C 29 (1984) 291.
[28] K.W. Schmid, F. Grümmer, A. Faessler, Phys. Rev. C 29 (1984) 308.
[29] K. Hara, Y. Sun, Nucl. Phys. A 529 (1991) 445.
[30] K. Hara, Y. Sun, Nucl. Phys. A 531 (1991) 221.
[31] K. Hara, Y. Sun, Nucl. Phys. A 537 (1992) 77.
[32] E. Caurier, K. Langanke, G. Martinez-Pinedo, F. Nowacki, Nucl. Phys. A 653 (1999) 439.
[33] L.M. Robledo, Phys. Rev. C 50 (1994) 2874.
[34] J.L. Egido, L.M. Robledo, Y. Sun, Nucl. Phys. A 560 (1993) 253.
[35] R. Rodrigues-Guzman, J.L. Egido, L.M. Robledo, Nucl. Phys. A 709 (2002) 201.
[36] J.L. Egido, L.M. Robledo, arhiv:nucl-th/0311106v1 28 Nov. 2003; Lect. Notes Phys., 641, (2004) 269.
[37] K.W. Schmid, Prog. Part. Nucl. Phys. 46 (2001) 145.
[38] A. Bohr, B.R. Mottelson, Nuclear Structure, Vol. II, Benjamin, Reading, 1975, (Chap. 4).
[39] A.A. Raduta, D.S. Delion, N. Lo Iudice, Nucl. Phys. A 551 (1993) 93.
[40] A.A. Raduta, A. Escuderos, E. Moya de Guerra, Phys. Rev. C 65 (2002) 024312.
[41] M.E. Rose, Elementary Theory of Angular Momentum, John Wiley & Sons, New York, 1957.
[42] A.A. Raduta, I.I. Ursu, D.S. Delion, Nucl. Phys. A 475 (1987) 439.
[43] N. Lo Iudice, A.A. Raduta, D.S. Delion, Phys. Rev. C 50 (1994) 127.
[44] A.A. Raduta, C. Sabac, Ann. Phys., NY 148 (1983) 1.
[45] A.A. Raduta, S. Stoica, N. Sandulescu, Rev. Roum. Phys. 29 (1984) 55.
[46] P. Möller, J.R. Nix, W.D. Myers, W.J. Swyatecki, At. Data Nucl. Data Tables 59 (1995) 185.
[47] A.A. Raduta, R. Budaca, A. Faessler, J. Phys. G: Nucl. Part. Phys. 37 (2010) 085108.
[48] A.A. Raduta, R. Budaca, A. Faessler, Ann. Phys., NY 327 (2012) 671.
[49] R. Budaca, A.A. Raduta, Rom. J. Phys. 57 (2012) 1088.
[50] http://www.nndc.bnl.gov/ensdf/.
[51] R. Tamisier, et al., Nuclear Phys. A 385 (1982) 430.
[52] B. Singh, A.R. Farhan, Nucl. Data Sheets 107 (2006) 1923.
[53] W.H.L. Moonen, et al., J. Phys. G: Nucl. Part. Phys. 19 (1993) 635.
[54] N.J. Stone, At. Data Nucl. Data Tables 90 (2005) 75–176.
[55] Yang Sun, Int. J. Mod. Phys. E 15 (2006) 1695.
[56] A.A. Raduta, R. Budaca, Phys. Rev. C 84 (2011) 044323.
[57] R. Budaca, A.A. Raduta, J. Phys. G: Nucl. Part. Phys. 40 (2013) 025109.
[58] H. Herold, et al., J. Phys. G: Nucl. Part. Phys. 7 (1981) 1467.
[59] A.A. Raduta, A. Escuderos, A. Faessler, E. Moya de Guerra, P. Sarriguren, Phys. Rev. C 69 (2004) 064321.
[60] A.A. Raduta, C.M. Raduta, A. Escuderos, Phys. Rev. C 71 (2005) 0244307.
[61] A.A. Raduta, C.M. Raduta, Phys. Lett. B 647 (2007) 265.
[62] C.M. Raduta, A.A. Raduta, Phys. Rev. C 76 (2007) 044306.